Agricultural and Forest Meteorology 149 (2009) 1327–1342

Contents lists available at ScienceDirect

Agricultural and Forest Meteorology

journal homepage: www.elsevier.com/locate/agrformet

Estimating volumetric surface moisture content for cropped soils using a soil wetness index based on surface temperature and NDVI

Kaniska Mallick [1], Bimal K. Bhattacharya *, N.K. Patel

Crop Inventory and Modelling Division, Agriculture-Forestry and Environment Group, Space Applications Centre (ISRO), Ahmedabad 380015, Gujarat, India

ARTICLE INFO

Article history:
Received 24 March 2008
Received in revised form 1 February 2009
Accepted 15 March 2009

Keywords:
Soil moisture
MODIS
ASTER
Optical–thermal
Agroecosystems
Comparison
Passive microwave

ABSTRACT

Surface soil wetness determines moisture availability that controls the response and feedback mechanisms between land surface and atmospheric processes. A study was carried out to estimate volumetric surface soil moisture content (θ_v) in cropped areas at field ($<10^2$ m) to landscape ($\leq 10^3$ m) scales. Triangular scatters from land surface temperature (LST) and normalized difference vegetation index (NDVI) space were utilized to obtain a soil wetness index (SWI), from which θ_v was derived, with the combination of dry and wet edges using data from ASTER (Advanced Space borne Thermal Emission and Reflection Radiometer) for field scale and MODIS (MODerate resolution Imaging Spectroradiometer) AQUA for landscape scale studies. The root mean square error (RMSE) of field scale θ_v estimates was higher (0.039 $m^3\ m^{-3}$) than that of the landscape scale (0.033 $m^3\ m^{-3}$). The narrow swath (~60 km) of finer resolution sensors (e.g. ASTER) often fails to capture the surface heterogeneity required in the triangle method for deriving SWI and could be one of the main reasons leading to relatively high error in θ_v estimates. At both the scales, the lowest error of θ_v estimates was found to be restricted within the NDVI range of 0.35–0.65. A geostatistical technique was applied to assess the influence of sub-pixel heterogeneity as an additional source of error for cross-scale comparison of θ_v estimates obtained from LST–NDVI scatters. The overall errors of θ_v estimates from LST–NDVI space were comparable with other globally available test results. The comparison of landscape scale θ_v from MODIS AQUA with large-area global estimates from a passive microwave sensor (e.g. AMSR-E) with longer microwave frequency (e.g. C-band) yielded 75% correlation and 0.027 $m^3\ m^{-3}$ root mean square deviation (RMSD) for fractional vegetation cover less than 0.5. The study recommends the synergistic use of shorter microwave frequency (e.g. L-band) and optical–thermal infrared bands as the best way of satellite based passive soil moisture sensing for vegetated surfaces.

1. Introduction

Near-surface soil moisture (0–0.05 m) is an important hydrological variable influencing the interactions between the land surface and atmospheric processes (Brubaker and Entekhabi, 1996). The partitioning of energy between sensible and latent heat fluxes is strongly controlled by surface wetness (Monteith, 1981; Shuttleworth, 1991; Entekhabi, 1995; Cahill et al., 1999; Dirmeyer et al., 2000). Through this control, soil moisture influences local weather variables, including boundary layer height and cloud coverage (Betts and Ball, 1998). It is important to understand these control and feedbacks when using global circulation models (GCMs) (Beljaars et al., 1996), regional climate models (Wetzel and Chang, 1988; Wilson et al., 1987), crop growth simulation models (de Wit and van Diepen, 2007; Guerif and Duke, 2000) and rainfall-runoff transformation models (Eltahir, 1998), for example. Despite the multi-dimensional importance of surface soil moisture, reliable regional and regular determination of this variable is extremely difficult through conventional point measurements, which are complex, expensive and available at a limited number of stations only.

A number of satellite-based techniques are in use for spatio-temporal soil moisture sensing. These utilize the electromagnetic spectrum in the optical–thermal and microwave bands. The latter has all-weather surface sensing capability in contrast to the former, which can sense only in clear skies. Passive microwave sensors (e.g. SSMI, AMSR-E) have 1–1.5 passes per day but have a coarse spatial resolution (~25 km). Therefore, the brightness temperature data from this type of sensors could be converted only to estimate large-area soil moisture as shown in a number of long term soil moisture mapping experiments such as SMEX02 (Cosh et al., 2004; Jacobs et al., 2004), SMEX03 (Jackson et al.,

* Corresponding author. Tel.: +91 79 26914377; fax: +91 79 26915823.
E-mail addresses: k.mallick@lancaster.ac.uk (K. Mallick), bkbhattacharya@sac.isro.gov.in (B.K. Bhattacharya).
[1] Present address: Department of Environmental Science, Lancaster Environment Centre, Lancaster University, LA1 4YQ, United Kingdom. Tel.: +44 01524 593894.

0168-1923/$ – see front matter © 2009 Elsevier B.V. All rights reserved.
doi:10.1016/j.agrformet.2009.03.004

2005), SMEX04 (Vivoni et al., 2008), SMOSREX (de Rosnay et al., 2006), SMACEX (Kustas et al., 2005) and soil moisture mapping missions like SMOS (Kerr et al., 2001), AMSR-E (Njoku and Li, 1999; Njoku et al., 2003), *IRS-P4* MSMR (Thapliyal et al., 2005), SSMI (Basist et al., 2001; Singh et al., 2005). However, active microwave sensors (SAR: Synthetic Aperture Radar) have higher spatial resolution (10–30 m), yet have low repeat intervals (once in 16–25 days). It is also known that SAR (e.g. ERS, ENVISAT) backscatter data in higher frequency (e.g. C-band) provide less accurate surface soil moisture estimates for vegetated or cropped fields than for bare ones.

Short-term variation of surface soil moisture in vegetated landscapes with greater spatial details can be frequently monitored only through optical–thermal infrared band data from moderate resolution (250 m to 1 km) sensors (e.g. MODIS TERRA and AQUA) having two overpasses per day. Sub-pixel soil moisture estimates in vegetated surface within a landscape could be obtained using data from similar bands with finer resolution (<100 m) satellite sensors such as Landsat or ASTER. Normalized difference vegetation index (NDVI), derived from red and near-infrared (NIR) bands, alone is not sensitive to short time soil moisture variations (Fensholt and Sandholt, 2003). However, the NIR-shortwave infrared (SWIR) based indices such as SIWSI (Fensholt and Sandholt, 2003), SASI (Khanna et al., 2007) have been found to capture soil wetness at 1 km resolution. The concept of using data from the thermal infrared (TIR) band to monitor canopy water stress was originally proposed by Jackson et al. (1977) who developed the crop water stress index (CWSI). A number of studies (Sandholt et al., 2002; Carlson, 2007; Nemani et al., 1993) have suggested that the combined information from land surface temperature (LST) and NDVI can provide better information on vegetation stress and moisture conditions at the surface. As a given area dries, it is expected that the negative relationship between NDVI and LST will be altered due to increased LST for the low NDVI areas. This leads to a triangular space that has been explored rigorously to extract surface soil moisture status (Carlson et al., 1995; Gillies and Carlson, 1995; Nemani et al., 1993; Smith and Choudhury, 1991; Goetz, 1997; Sandholt et al., 2002). An overview of the LST–NDVI 'triangle method' for estimating soil surface wetness can be found in Carlson (2007).

Surface soil moisture content can also be potentially derived from estimates of surface thermal inertia. The feasibility of using apparent thermal inertia (Rosema and Fiselier, 1990; Stisen et al., 2008) from noon–night LST difference or morning rise in LST to estimate surface soil moisture at coarser scales (2–8 km) was demonstrated (Wetzel and Woodward, 1987; Hayden et al., 1996; Verstraeten et al., 2006) using optical and thermal data from geostationary sensors. This technique has limitations due to variable cloud cover conditions between day and night or two different hours within daytime. The most convenient approach would be to extract surface soil wetness using optical-TIR band data from the same overpass. The LST–NDVI space was, therefore, utilized in the present study to derive surface soil wetness (i) to estimate volumetric soil moisture content followed by validation with *in situ* measurements in cropped soils at both field ($<10^2$ m) and landscape ($\leq 10^3$ m) scales; (ii) to compare soil moisture estimates at these two different scales and (iii) finally to compare landscape scale estimates with global large-scale soil moisture from passive microwave sensor.

2. Surface temperature–vegetation index space

2.1. Theory and hypothesis

Land surface temperature largely depends on soil moisture and fractional vegetation cover. However, no universal and direct relation between LST and soil moisture is evident. Several workers (Stisen et al., 2008; Wang et al., 2006) demonstrated the physical relationship between vegetation index (e.g. NDVI) and LST in the form of a scatterplot, which could be a triangular variant of trapezoidal space. This implies that the sensitivity of LST to soil moisture differs for the canopy and for the soil surface beneath the plants. This sensitivity to soil moisture content tends to be much greater for bare soil than for canopies. This association between LST and NDVI, therefore, allows estimation of soil moisture content.

The following mechanisms are suggested as those determining the location of a pixel in the LST–NDVI space. These are based on the earlier findings reported in the literature (Sandholt et al., 2002; Carlson, 2007). The fractional vegetation cover can be related to spectral vegetation indices such as NDVI. This influences the amount of bare soil and vegetation visible to a sensor and differences in radiative temperature between the soil and canopy will affect the spatially integrated LST. Evapotranspiration largely controls the surface temperature as it is a term in the surface energy balance, which stipulates that

$$R_n = \mathrm{LE} + H + G \quad (1)$$

where R_n is the net radiation, LE is the evapotranspiration, H is the sensible heat flux and G is the soil heat flux (all fluxes in W m^{-2}). The surface temperature plays a key role in all of these fluxes.

The lower LE, the more energy available for sensible heating of the surface, H. Stomatal resistance to transpiration is a key factor, which is partly controlled by soil moisture availability. Thermal inertia (a thermal soil property which combines heat capacity and thermal conductivity, see e.g. Murray and Verhoef, 2007) influences LST in the case of partly vegetated surfaces, as they affect the amount of heat transferred into the soil, G. These thermal properties are a function of soil type and change with surface soil moisture (Verhoef et al., 1996). The available energy incident at the surface ($R_n - G$) also affects LST. The radiative control of LST implies that areas with a lower net shortwave radiation balance (e.g. due to a high albedo) will have lower temperatures, all else equal. Albedo is controlled by soil type, surface soil moisture, and vegetation cover. Incident radiation also affects the stomatal resistance to transpiration, which factors into the partitioning of net radiation into sensible and latent heat. The ability to transfer heat away from the surface into the atmosphere is an important component in the control of LST. This, in part, explains how vegetated surface with higher roughness length have lower LST (all else equal) compared to bare soil, which influences the shape of the LST/NDVI space. Similarly, homogeneous surfaces with unlimited water supply (for instance, irrigated surfaces) may have higher LST than expected, if turbulent exchange is reduced by poor mixing (Nemani and Running, 1997).

The conceptual LST–NDVI triangular space, with LST (y-axis) plotted as a function of NDVI (x-axis) is shown in Fig. 1. The hypotenuse of the triangle represents a warm/dry edge consisting of a group of points indicative of zero surface soil wetness for different NDVI classes in contrast to the cold/wet edge represented by the base of the triangle having maximum surface soil wetness conditions at different NDVI classes. The left edge represents bare soil ranging from dry to wet (top-down). For bare soils, at constant irradiance, LST is primarily determined by soil moisture content, via evaporative control and thermal properties of the surface. As the green vegetation increases along the x-axis (with NDVI), the maximum LST (=$\mathrm{Ts}_{\max}$) decreases. For dry conditions, the negative relation is defined by the warm/dry edge, which is the upper limit of LST for a given surface type and climate forcing. The 'wet' edge consists of a group of points

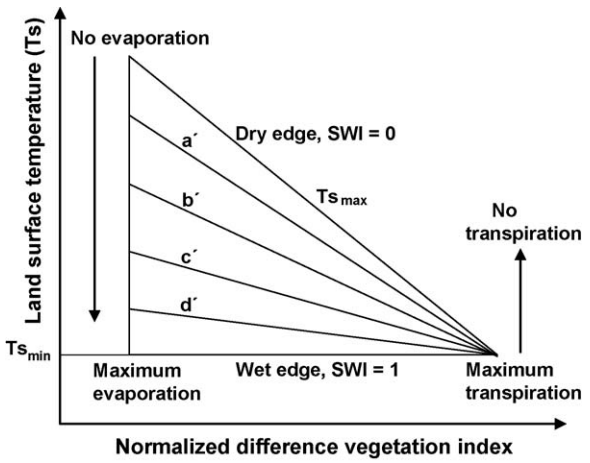

Fig. 1. Conceptual diagram of LST–NDVI triangle for determining soil wetness index. The value of SWI is zero along the dry edge and its value is 1 along the wet edge. The intermediate SWI isolines at 0.2, 0.4, 0.6 and 0.8 are represented by a′, b′, c′ and d′, respectively.

forming a horizontal or sloping line (at the level of Ts_{min}) for different surface types or fractional cover.

Stisen et al. (2008) explained the difference between the 'theoretical' and 'observed' dry edges in the triangle while estimating evapotranspiration using difference LST (from morning rise) and NDVI space. The theoretical dry edge represents zero surface soil wetness and zero evapotranspiration, since LST reaches a physical maximum when no evaporative cooling occurs. In this case, complete stomatal closure occurs for the vegetated part (Moran et al., 1994). In reality, zero evapotranspiration rarely occurs for dense vegetation covers even in semi-arid environments, primarily due to soil water uptake from the root zone and also due to the spatially integrated nature of satellite observations. Consequently, the dry edge observed in remote sensing data is characterized by lower temperatures than the theoretical dry edge and is, therefore, not assigned zero evapotranspiration. In that way, surface soil wetness is decoupled from the root zone soil wetness in vegetated pixels.

2.2. Assumptions and uncertainties

The LST–NDVI approach is valid when both minimum and maximum surface soil wetness can be observed within the geographical extent of the study area. This assumption requires a heterogeneous study area with uniform atmospheric forcings. The sources of uncertainties in operational soil wetness estimation from LST–NDVI triangle are:

(i) View angle effects on LST and NDVI are not considered.
(ii) The triangle may not be fully determined if the area of interest does not include a full range of land surface types and conditions (e.g. dry bare soil, saturated bare soil, water stressed vegetation and well watered vegetation).
(iii) Cloud shadows are not accounted for.
(iv) Errors in LST and NDVI retrieval from satellite data may propagate due to unknown and varying land surface emissivity and atmospheric effects.
(v) The influence of soil wetness in deeper layers (Capehart and Carlson, 1997) on top soil layers is not accounted for.
(vi) Dependence of LST and NDVI on surface type, due to differences in aerodynamic resistance (Friedl and Davis, 1994; Lambin and Ehrlich, 1995), is not considered.

3. Characteristics of the study region

Different agricultural regions, spread over four Indian states: Punjab, Haryana, Karnataka and Orissa, were selected for *in situ* soil moisture measurements to validate surface (0.05 m) soil moisture estimates using satellite data (see Table 1 for a list of these regions and their coordinates, as well as agroclimatic characteristics). Representative crops over these study regions were wheat (Punjab and Haryana) in *rabi* (November–April) season, cotton (Haryana) in *kharif* (June–October), *rabi* sorghum (Karnataka) and *rabi* groundnut (Orissa). The studied crops represent a wide variety of crop groups such as cereals (e.g. wheat), millets (e.g. sorghum), oilseeds (e.g. groundnut), fibres (e.g. cotton), differing largely in canopy architecture, phenological development and physiological response to agroclimatic conditions. The regions represent a wide variety of soil types. Predominant soil textures are sandy loam both in Punjab and Haryana, sandy clay loam in Orissa and clay loam in Karnataka. Ratio (R/PE) of cumulative annual rainfall (R) and pan evaporation (PE) varied between 0.22 and 1.18. Wheat crops in Punjab and Haryana receive four irrigations throughout the growing season. However, *rabi* groundnut and sorghum are grown in residual soil moisture conditions. Cotton is generally grown as a rainfed crop.

Table 1
Agroclimatic characteristics of the study regions.

Study regions	Central co-ordinates		Agroclimatic region	Cropping pattern	Soil type	R/E
	Longitude	Latitude				
(a) Punjab						
Ludhiana	75°40′E	30°50′N	TGPR	Rice–wheat	New alluvial	0.38
Moga	75°05′E	30°49′N				
Ferozpur	74°47′E	30°52′N				
Jalandhar	75°46′E	31°05′N				
Kapurthala	75°11′E	31°33′N				
Amritsar	74°57′E	31°35′N				
Patiala	76°32′E	30°25′N				
(b) Haryana						
Hissar	75°42′E	29°17′N	TGPR	Cotton–wheat	New alluvial	0.22
(c) Orissa						
Dhenkanal	85°48′E	20°52′N	EPHR	Fallow–groundnut	Laterite	1.18
(d) Karnataka						
Bijapur	75°35′E	16°50′N	SPHR	Fallow–sorghum	Black soil	0.25

LGPR: Lower Gangetic Plains Region; TGPR: Trans-Gangetic Plains Region; EPHR: East-coast Plains & Hills Regions; SPHR: Southern Plateau & Hills Region; GPHR: Gujarat Plains and Hills Region. R/E: Annual rainfall (mm)/Annual pan evaporation (mm).

4. Observations and datasets

4.1. Satellite data

Optical and thermal infrared band data from two different polar orbiting satellite sensors, ASTER (Advanced Space-borne Thermal Emission and reflection Radiometer) and MODIS (MODerate Resolution Imaging Spectroradiometer) AQUA, were used to estimate volumetric surface soil moisture at 0.0009° (field) and 0.01° (landscape) scales, respectively. Level 3 products on land surface temperature at 90 m spatial resolution and normalized difference vegetation index at 15 m spatial resolution from ASTER were used. The data were acquired from Earth and Remote Sensing Data Archival Centre (ERSDAC), Japan (http://imsweb.aster.ersdac.or.jp/) in Transverse Mercator (TM) projection with dimensions of 830 rows and 700 columns. Two clear scenes of ASTER covering Ludhiana district and some of its adjacent parts in Punjab were acquired for DOY (day of year) 323 (18 November 2004) and 339 (4 December 2004), respectively. Tiles of MODIS AQUA daily LST V004 product (MYD11Q1) at 927 m spatial resolution and seven band surface reflectance product (MYD09Q1) at 463 m spatial resolution in Integerised Sinusoidal (ISIN) projection were acquired through EOS data gateway (http://lpsaac.usgs.gov) for all the dates corresponding to clear sky soil moisture sampling between 2004 and 2006 (for Orissa, 2003–2006). Soil moisture estimates from MODIS AQUA and ASTER were resampled at 0.01° and 0.0009° grids, respectively, to fit the LST grid.

Global spatial product of volumetric surface soil moisture at 0.25° grid generated with observations from C-band passive microwave radiometer, AMSR-E (Advanced Microwave Scanning Radiometer) onboard AQUA platform was used for comparing estimates from optical–thermal band combinations. Retrieved volumetric surface soil moisture data from AMSR-E were acquired from National Snow and Ice Data Center (NSIDC), University of Colorado, Boulder for the crop growth period between November 2005 and May 2006. These were then subjected to georegistration through geometric look-up table (GLT) that was generated using latitude and longitude information. One ascending pass of AMSR-E is able to cover 80% of Indian landmass. The native projection was Cylindrical Equal Area with pixel resolution of approximately 25 km.

4.2. In situ measurements

Soil moisture measurements were carried out at 14-day intervals during first and third week of each month between October 2004 to April 2005 and October 2005 to April 2006 in all the four study regions with *rabi* crops. In addition, soil moisture sampling was also carried out during October 2003 to April 2004 in Orissa and in a cotton crop during two *kharif* seasons (May to October in 2004 and 2005) in Haryana. An interval of 14 days was kept to take into account a shift in phenological stage. Soil moisture was measured at 0.025 m depth gravimetrically, except in Punjab where a calibrated roving Time Domain Reflectometer (TDR: model SDEC, France) was used to obtain measurements over a larger number of locations. Homogeneous crop patches of 1 km × 1 km each were selected within central locations of all the study regions. Each square sampling patch was divided into four 500 m × 500 m squares. Soil sampling points were located at four corners of each square, plus one at its centre. There were 13 such sampling points to represent MODIS AQUA footprint area (927 m × 927 m) of one pixel. For validation of ASTER (90 m resolution) based soil moisture estimates, point measurements in the center of each 90 m pixel were used. All measurements were carried out between 12:00 and 14:00 h LMT (local mean time) corresponding to equatorial crossing time of MODIS AQUA between 13:00 and 13:30 h. Soil moisture measured at 12:00 h was used for validating ASTER estimates since its equatorial crossing time varied between 10:45 and 11:30 h.

5. Methodology

5.1. Soil wetness index (SWI) from LST–NDVI triangle

In LST–NDVI triangle (Fig. 1), highest LST (Ts_{max}) along the dry edge represents the driest surface soil conditions when surface soil wetness is zero. The wettest (saturated) soil conditions are represented through the minimum LST (=Ts_{min}) along the 'wet edge' when surface soil wetness is the highest. It is assumed that moisture availability varies linearly from the dry edge to the wet edge. This is in agreement with previous interpretations of LST–NDVI space (Carlson, 2007; Stisen et al., 2008). A soil wetness index (SWI) on a given day or time (t), representing relative surface soil moisture, is defined as:

$$\mathrm{SWI}(t) = \frac{\mathrm{Ts}_{\mathrm{max(i)}} - \mathrm{Ts}_{\mathrm{(i)}}}{\mathrm{Ts}_{\mathrm{max(i)}} - \mathrm{Ts}_{\mathrm{min}}} \quad (2)$$

where, $Ts_{(i)}$ is the land surface temperature of i-th pixel. Ts_{min} is the minimum LST in the triangle that defines the wet edge. $Ts_{max(i)}$ is the maximum LST for i-th NDVI. Carlson (2007) objectively determined the dry edge as the least square fit to NDVI using a polynomial (of the 3rd or 4th order) using fine resolution thermal data as well as simulated data from Soil Vegetation Atmosphere Transfer model runs. In the present study, most of the LST–NDVI scatters from 927 m spatial resolution showed a clear triangle with prominent linear dry edge and horizontal wet edge. The LST–NDVI scatters at 90 m pixel resolution showed a non-linear trend along the dry edge at higher NDVI values and a sloping wet edge. However, to keep the simplicity and uniformity in approach across different scales, the dry edge was modelled via a linear empirical fit to NDVI:

$$\mathrm{Ts}_{\mathrm{max(i)}} = a + b\mathrm{NDVI}_i \quad (3)$$

Here, NDVI is the normalized difference vegetation index of the i-th pixel, 'b' is the slope and 'a' is the intercept of the linear dry edge. Ts_{max} values for different NDVI classes were extracted with a NDVI interval of 0.05. Then 'dry edge' parameters were estimated through regression analysis. The 'wet edge' is the horizontal line represented by Ts_{min}.

Along the dry edge, SWI = 0, whereas it equals 1 along the wet edge. Isolines (a′, b′, c′ and d′) of SWI in Fig. 1 represent equal surface moisture availability. By knowing the upper (θ_{max}) and lower (θ_{min}) limits of volumetric soil moisture at the surface, the wetness index (SWI) on a given day or time can be converted to an absolute estimate of volumetric surface soil moisture (θ_v) using the following relationship (Wagner et al., 1999)

$$\theta_v = \theta_{\mathrm{min}} + \mathrm{SWI}(t)(\theta_{\mathrm{max}} - \theta_{\mathrm{min}}) \quad (4)$$

θ_{max} is the upper limit of θ_v and can take on values between field capacity (FC) and saturated moisture content. In most cases, except immediately after a heavy rainfall event or irrigation, θ_{max} can be set equal to FC. For more practical purposes θ_{max} can be represented as arithmetic mean of FC and maximum retentive capacity (Thapliyal et al., 2005; Verstraeten et al., 2006). The θ_{min} is the lower limit of θ_v and can be represented as permanent wilting point (PWP). These limits are soil type specific. The difference ($\theta_{max} - \theta_{min}$) between these two represents total water capacity (TWC) of soil.

5.2. Calibrating soil moisture limits

Wetness was generated using LST–NDVI scatter from ASTER LST and resampled NDVI at 90 m for DOY 323 (18 November 2004) and

Table 2
List of DOY of *in situ* soil moisture measurements.

Study regions	Training/calibration datasets			Validation datasets		
	2003	2004	2005	2004	2005	2006
Punjab	N.A.	283, 299, 308, 331, 345, 363	34, 61, 102	N.A.	320, 340, 342	23, 57, 58, 59, 86, 87
Haryana	N.A.	38, 57, 71, 86, 97, 112, 142, 246, 280, 309	N.A.	N.A.	7, 20, 32, 62, 74, 96, 111, 264, 292, 321	52, 76
Orissa	339, 345	14, 42, 56, 70, 83	N.A.	342, 356	4, 19, 33, 48, 61, 75, 97, 322, 340, 354	3, 20, 36, 50, 65, 79
Karnataka	N.A.	294	62, 76, 292	N.A.	319, 340, 356	3, 17, 38, 52, 68, 81

N.A.: not available; DOY: day of the year.

339 (4 December 2004) in Ludhiana district of Punjab. MODIS AQUA LST data at 927 m resolution and surface reflectance data at 463 m resolution were used to estimate SWI at 927 m. Datasets were divided into two parts: (a) training datasets and (b) validation datasets. Training datasets were used to calibrate SWI with *in situ* θ_v. The upper (θ_{max}) and lower (θ_{min}) limits of surface soil moisture content mentioned in Eq. (4) were obtained for all the four study regions through calibration. These limits were then applied to independent MODIS AQUA datasets to estimate θ_v. The days of training or calibration and validation of MODIS AQUA datasets are summarized in Table 2. Since soil moisture limits are soil type specific but time-invariant, the same regional limits were applied to coinciding ASTER derived SWI.

The coefficients of least square regression between θ_v and SWI were used to derive upper (θ_{max}) and lower (θ_{min}) soil moisture limits over study regions. These are soil type specific and do not vary over a large spatial extent. The limits over four study regions are given in Table 3. The upper limits were found to be 0.31, 0.29, 0.31 and 0.41 $m^3\ m^{-3}$, in Punjab, Haryana, Karnataka and Orissa, respectively. The lower limits were 0.012, 0.020, 0.002 and 0.076 $m^3\ m^{-3}$, respectively. The TWC was found to vary between 0.27 and 0.34 $m^3\ m^{-3}$ for coarser texture (e.g. sandy loam) soil having less organic carbon in Hissar, Haryana, to finer texture (e.g. sandy clay loam) soil containing higher levels of organic carbon in Dhenkanal, Orissa. These limits were compared (last column in Table 3) with texture-based limits reported by the Food and Agricultural Organization (FAO) based on global soil samples (FAO/UNESCO, 1974). Sandy loam soil is predominant both in Punjab and Haryana but total water capacity was less in Haryana. Two factors could have lead to the above differences: (i) the proportion of sand is more (75%) in Haryana than that over Punjab (55%); (ii) organic carbon content is also higher in Punjab, which as a result improves soil aggregation and TWC. Since TWC taken from the FAO global soil database is only based on soil textural classes, no difference in TWC was found from FAO limits between these two states. Maximum TWC was obtained through present calibration over Orissa, because it contains maximum organic carbon (0.78%). Karnataka contains a higher proportion of clay (57%) than Orissa (37%), differences in organic carbon content must have led to better soil aggregation and higher TWC in Orissa than in Karnataka. The Global database from FAO reported higher TWC in clayey soil and lower values in sandy loam soil. It does not consider soil organic carbon content to define the limits. The present methodology takes account of soil aggregation properties in addition to soil texture through θ_v–SWI relation and is thus used to calibrate the soil moisture limits at the scale of satellite observations. Therefore, the same limits in the present study were further used to invert to θ_v from independent wetness datasets over the same regions.

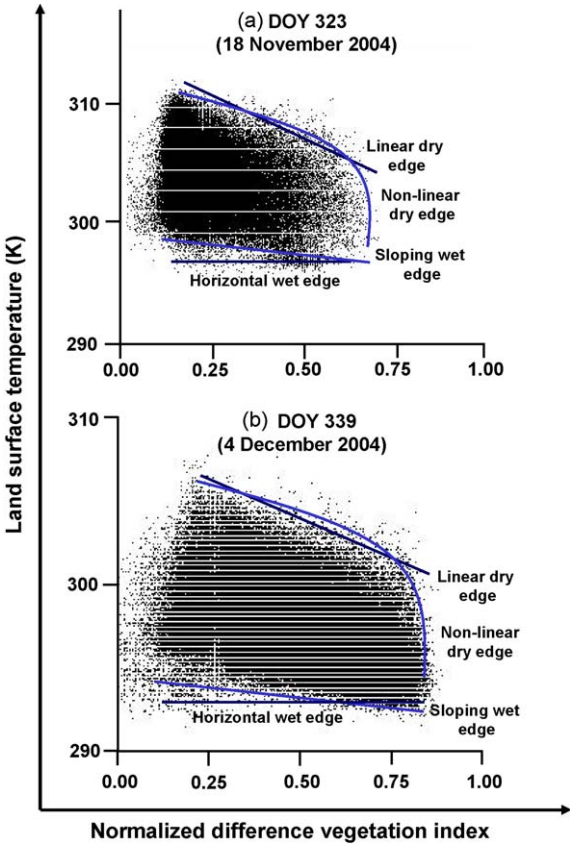

Fig. 2. LST–NDVI scatterplots from ASTER over Punjab on two clear winter days.

Table 3
Calibrated soil moisture limits (θ_{max}, θ_{min}) and comparison of calibrated total water capacity (TWC) with that computed from FAO soil moisture limits.

Study regions	Soil texture			Organic carbon (%)	Calibrated upper soil moisture limit (θ_{max})	Calibrated lower soil moisture limit (θ_{min})	Correlation coefficient (r)	TWC ($m^3\ m^{-3}$) (calibrated)	TWC ($m^3\ m^{-3}$) (FAO)
	Sand (%)	Silt (%)	Clay (%)						
Ludhiana, Punjab	55	33	12	0.60	0.313	0.012	0.77	0.301	0.326
Hissar, Haryana	75	12	13	0.50	0.291	0.022	0.97	0.269	0.326
Dhenkanal, Orissa	39	24	37	0.78	0.414	0.076	0.94	0.338	0.292
Bijapur, Karnataka	27	16	57	0.58	0.310	0.002	0.94	0.308	0.321

Total water capacity (TWC) = $\theta_{max} - \theta_{min}$. Here, θ_{min}: volumetric soil moisture content ($m^3\ m^{-3}$) at permanent wilting point (PWP). θ_{max}: arithmetic mean of volumetric soil moisture content ($m^3\ m^{-3}$) at saturation and field capacity (FC).

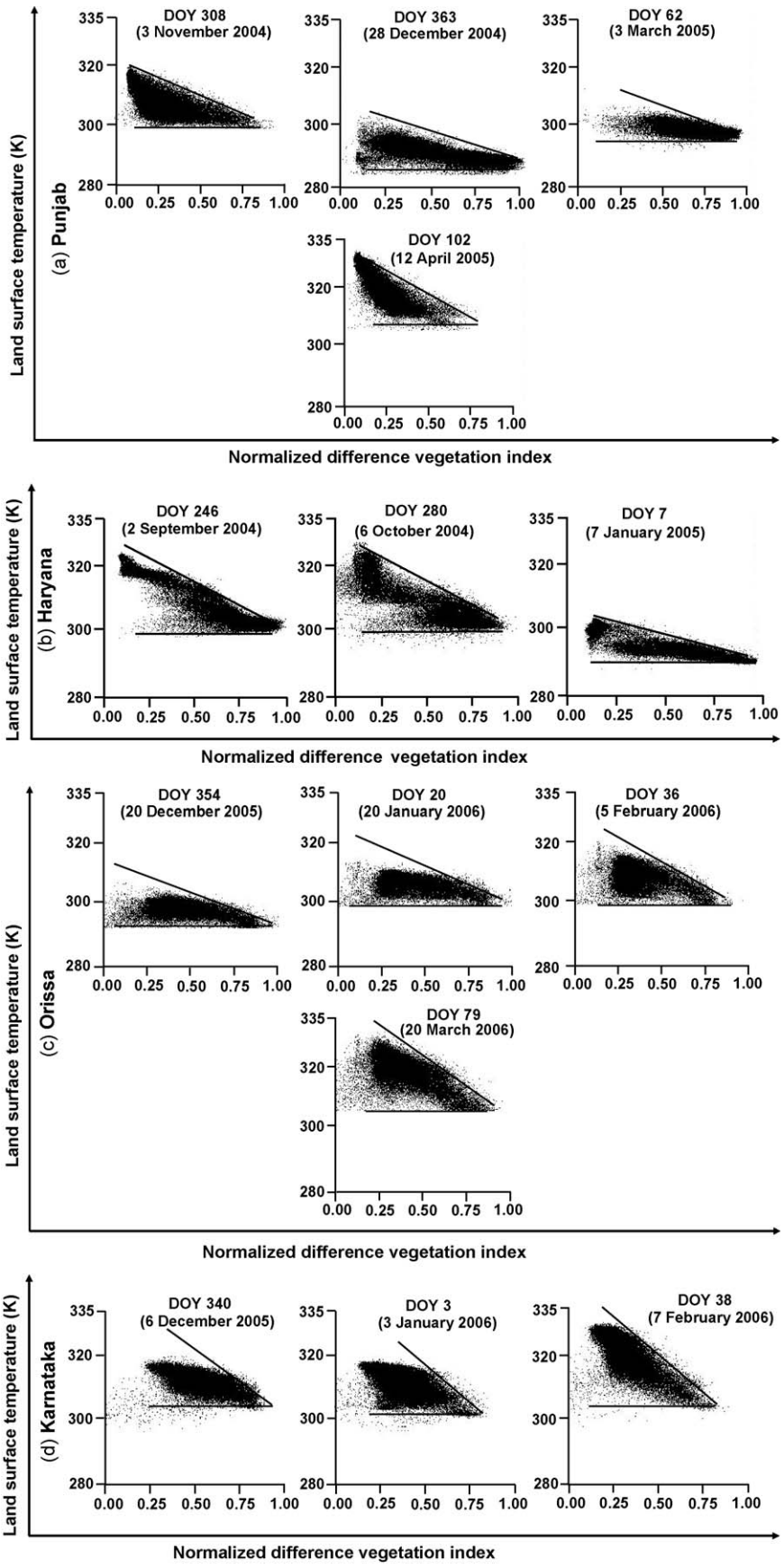

Fig. 3. Some illustrative examples of LST–NDVI scatterplots from MODIS AQUA over four different study regions.

6. Results and discussion

6.1. LST–NDVI scatterplots

The dry and wet edges were determined from LST–NDVI scatterplots to generate surface soil wetness over the study domain and its subsequent conversion to volumetric soil moisture content. The finer resolution (90 m) ASTER data having narrow swath (60 km) are governed by in-field surface heterogeneity. The size of the sampling window for LST–NDVI scatter was, therefore, kept at 50 km × 50 km, to extract wetness from a narrower swath. However, a larger sampling domain may be required to capture the desired wetness pattern in some cases when LST and NDVI spatial dynamics were narrow. Given the larger swath (2330 km ± 55° cross-track) with moderate resolution (927 m) MODIS AQUA sensor, a larger sampling window of 100 km × 100 km was imposed to capture landscape heterogeneity in all the cases. It is also assumed that the daily averages of key atmospheric variables did not exhibit much variability for clear skies within the spatial extent of 100 km × 100 km (Mueller et al., 2004). The illustrative examples of LST–NDVI scatterplots from ASTER and MODIS AQUA are shown in Fig. 2 and Fig. 3, respectively. The group of points along the dry edge for ASTER LST–NDVI scatterplots displayed a non-linear trend on both the DOYs (323 and 339) (Fig. 2a and b) at NDVI values more than 0.40. A sloping wet edge was prominent on both dates. In the sloping dry edge of the scatter, pixels with higher NDVI (>0.4) and low temperatures represent the asymptotic region in which the temperature approaches that for a sunlit canopy at field scale. At this end of the dry edge, the upwelling longwave radiation from the soil is almost totally attenuated (Carlson et al., 1990). Moreover, the electro-magnetic radiation (EM) at near-infrared wavelength region can penetrate approximately eight leaf layers and reflected back as total internal reflection, while it penetrates only one leaf layer or less at the red wavelength region because of the strong chlorophyll absorption near 0.67 μm (Lillesaeter, 1982). As a result, NDVI approaches a saturation level asymptotically for LAI ranging between 2 and 6, depending on vegetation types and environmental conditions (Carlson and Ripley, 1997) and this effect is more pronounced at field scale with finer resolution satellite (e.g. LANDSAT, ASTER) data. Frequency distribution of NDVI on DOY 323 (18 November 2004) showed that the majority of pixels had NDVI values between 0.13 and 0.45 (Fig. 4a) that corresponds to low crop cover conditions between fallow (after rice harvesting) to emergence (e.g. wheat). On the other hand, well-distributed NDVI values (0.25–0.70) were found on DOY 339 (4 December 2004), which could be due to more foliage of wheat (Fig. 4b). LST of the majority of pixels were within 293–308 K having a slightly higher spread (9 K) on DOY 323 compared to 339 (7 K) (Fig. 4c and d).

Some illustrative examples of LST–NDVI scatterplots from MODIS AQUA over four study regions are shown in Fig. 4 for (a) Punjab (b) Haryana (c) Orissa and (d) Karnataka. As compared to ASTER (Fig. 2a and b), a greater dynamic range of LST, of the order of 19–21 K (i.e. between 297–318 K and 285–304 K, respectively) was evident during early November and late December in Punjab with MODIS AQUA scatters, while a well-distributed NDVI was evident in all the scatters. A clear triangular pattern was visible for all scatterplots. The stronger influence of lumped canopy at landscape scale smoothed out the non-linear distribution of LST at higher NDVI values along the limiting edges as opposed to greater influence of sunlit-shaded canopy at field scale leading to non-linear dry and wet edges. In addition, the effect of asymptotic increase of NDVI followed by saturation at LAI between 2 and 6 is relatively less prominent with lumped canopy at landscape scale (Carlson and Ripley, 1997). In Haryana, a larger divergence in the triangular scatters (Fig. 3b) was found on DOY 247 (3 September 2004) and 280 (6 October 2004), as compared to a narrower distribution on DOY 7 (7 January 2005). The rainfed cotton crop is generally grown as the dominant crop in the study region during

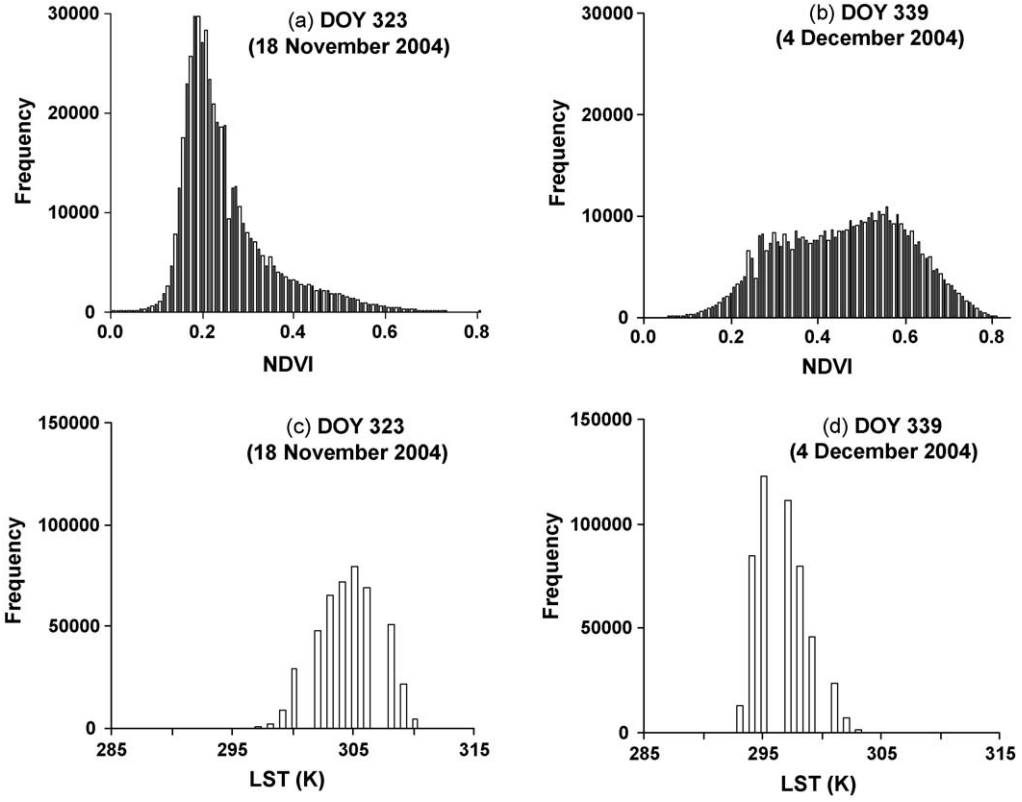

Fig. 4. Frequency distribution of NDVI and LST from ASTER data over Punjab coincident to two *in-situ* measurement dates.

May to October. The spatially varying soil wetness which largely depends on distribution of southwest monsoon rainfall and large canopy heterogeneity in cotton crops due to their branching habit must have resulted into a flattened LST–NDVI distribution. The relatively uniform canopy of cereal crops such as wheat grown during November to April with 3–4 irrigations led to a narrower distribution. In Orissa, the slope of the triangle of scatterplots increases between December and March (Fig. 3c). The *rabi* crop (e.g. groundnut) is grown during this period with residual moisture after southwest monsoon rainfall recedes. This caused variable surface drying for different canopy cover fraction. In Karnataka (Fig. 3d), a gradual transition towards a well-distributed scatter of points with sharp linear dry edge and horizontal wet edge was found between DOY 340 (6 December 2005) to 38 (7 February 2006). The *rabi* sorghum, being the dominant crop, is grown in residual soil moisture after the withdrawal of the south-west monsoon. This leads to differential soil drying in relation to canopy heterogeneity.

Temporal variation of dry edge slope, intercept and Ts_{min} extracted from LST–NDVI scatterplots for *in situ* moisture measurement days are shown in Fig. 5 for (a) Punjab; (b) Haryana; (c) Orissa and (d) Karnataka. The slope of the dry edge showed little variation in Punjab (Fig. 5a), around −20 K, except in a few cases when it reached values of around −10 and −40 K. However, a larger fluctuation occurred in dry edge intercepts, with values ranging between 310 and 335 K. In Haryana (Fig. 5b) and Karnataka (Fig. 5d), a larger fluctuation in slope was observed. It varied between −18 and −100 K in Haryana and −19 and −58 K in Karnataka. Similar to the findings for the dry edge slope, a large variation in the intercept, between 310–355 K and 320–355 K, respectively, in both study regions, was also evident. In Orissa (Fig. 5c), a cyclic variation in both dry edge slope (between −10 to

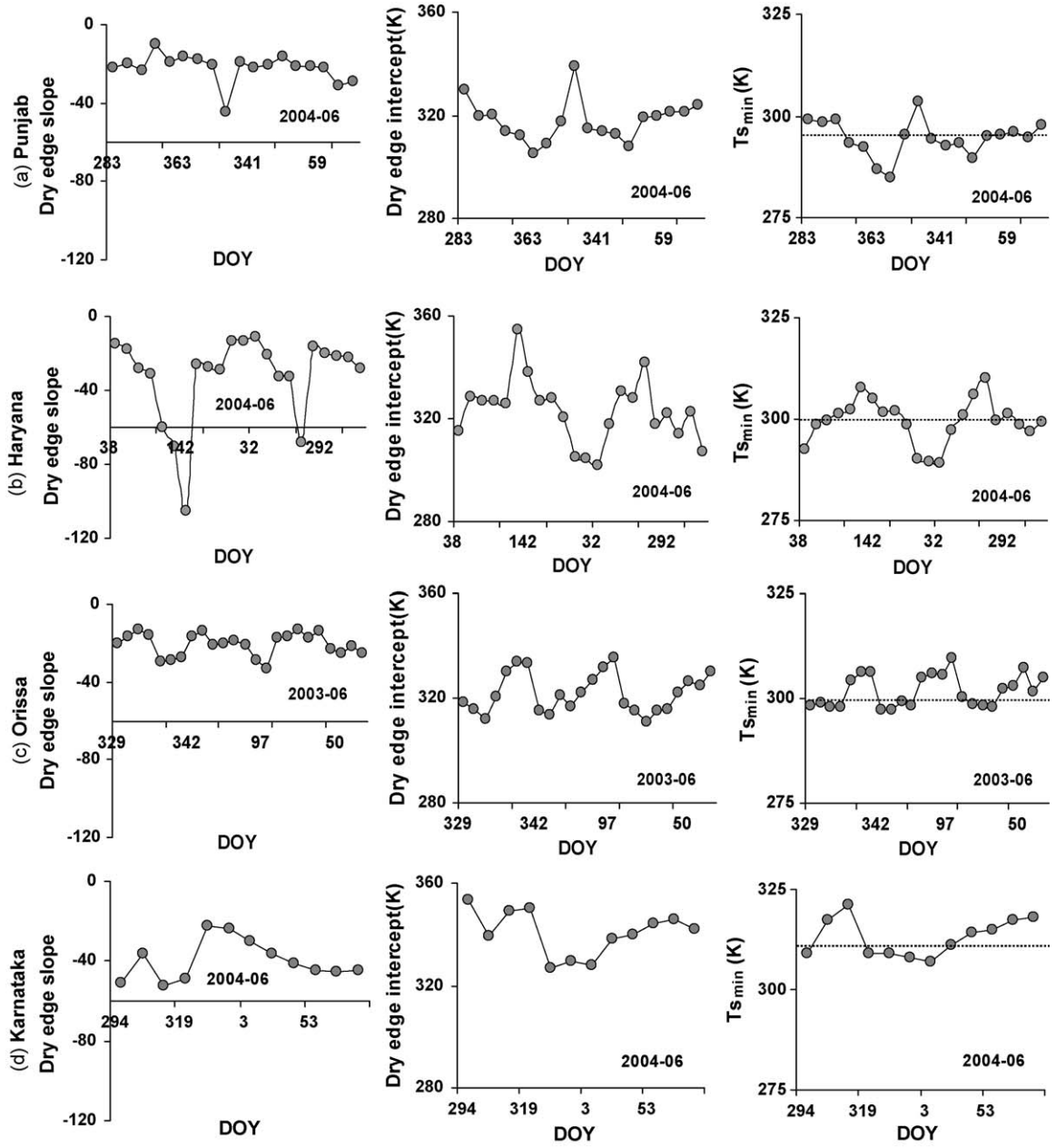

Fig. 5. Temporal variation of dry edge slope, intercept and Ts_{min} (dotted line represents the average Ts_{min}) over four different study regions as obtained from LST–NDVI triangle of MODIS AQUA. DOY means day of the year.

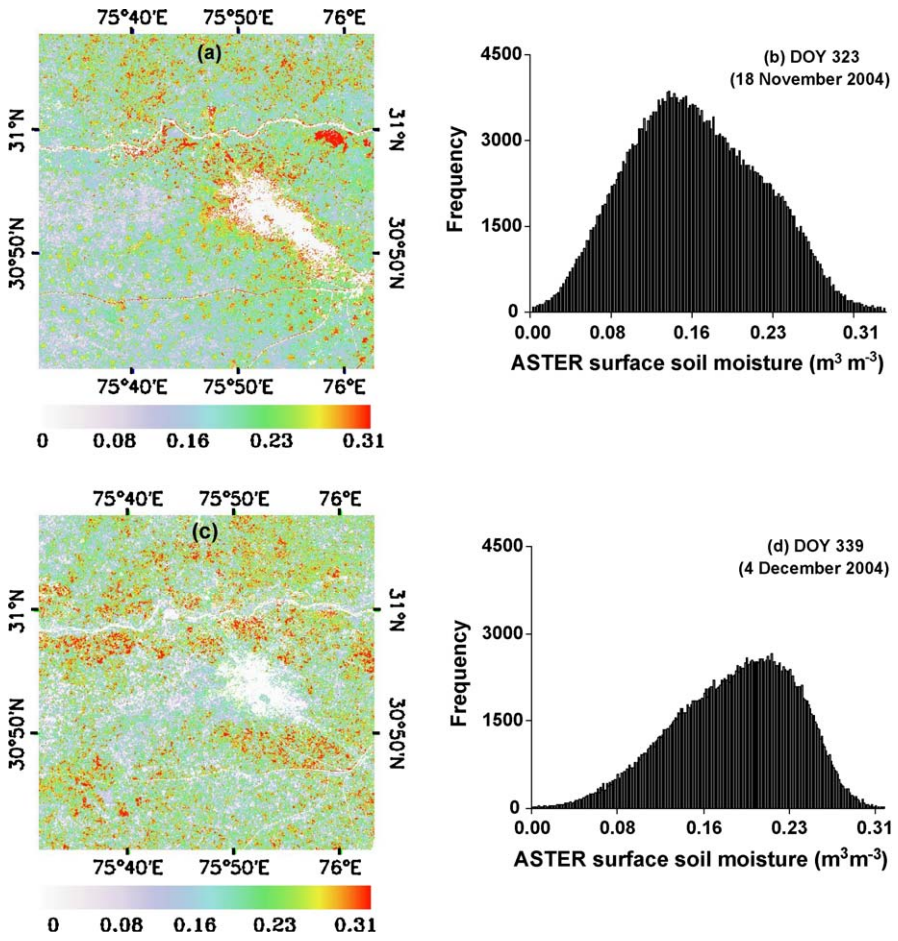

Fig. 6. (a) Spatial distribution of field scale soil moisture on DOY 323 (18 November 2004) in Ludhiana, Punjab using ASTER SWI; (b) frequency distribution of field scale surface soil moisture on DOY 323 (18 November 2004) in Ludhiana, Punjab using ASTER SWI; (c) spatial distribution of field scale soil moisture on DOY 339 (4 December 2004) in Ludhiana, Punjab using ASTER SWI; (d) frequency distribution of field scale surface soil moisture on DOY 339 (4 December 2004) in Ludhiana, Punjab using ASTER SWI.

−30) and intercept (315–335 K) was observed. In Punjab, *rabi* crop is grown during November to April with 3–4 irrigations applied at different times depending on location. This led to a relatively flat dry edge slope and wider variation in the intercept. Different growth characteristics with respect to water availability for a rainfed crop followed by an irrigated crop in Haryana, a *rabi* crop grown in residual moisture in Karnataka, and a rainfed crop followed by *rabi* groundnut grown in residual moisture in Orissa, could have led to a wider variation in both dry edge slope and intercept as compared to Punjab. Differences in the fluctuations in Ts_{min} (Punjab: 285–300 K, Haryana: 287–307 K, Karnataka: 307–320 K, Orissa: 297–307 K) about the mean line were also observed across four study regions. Thus, the dry edge parameters and wet edge from LST–NDVI scatterplots clearly distinguished the growing conditions, in terms of surface wetness, among different agroecosystems.

6.2. Validation of surface soil moisture estimates

6.2.1. Field scale

Soil moisture estimation at field scale (0.0009°) was carried out for two DOYs (323 and 339) only over Punjab by using region-specific calibrated upper and lower θ_v limits and SWI generated from ASTER (90 m) NDVI and LST. It was found that the mean value of *in situ* surface soil moisture was lower (0.177 $m^3\ m^{-3}$ with CV 27.8%) on DOY 323 as compared to 0.204 $m^3\ m^{-3}$ (with CV 29.3%) on DOY 339. The spatial distributions of field scale θ_v and their histograms on 18 November (DOY 323) and 4 December (DOY 339) are shown in Fig. 6a–d, respectively. Substantial differences in soil moisture pattern were evident between these two with relatively higher moisture on DOY 339 due to irrigation applied coincident to wheat sowing. The majority of pixels (53%) on 18 November (Fig. 6a and c) were within lower θ_v class of 0–0.15 $m^3\ m^{-3}$, whereas, on 4 December (Fig. 6b and d), the majority of pixels (65%) correspond to higher θ_v class, 0.151–0.25 $m^3\ m^{-3}$. Error statistics of θ_v estimates for different moisture classes and pooled datasets are given in Table 4. The mean bias, mean absolute error (MAE) and root mean square error (RMSE) were −0.016, 0.026 and 0.039 $m^3\ m^{-3}$ (20% of measured mean) over pooled datasets with correlation coefficient (r) 0.76. However, more errors (28% of measured mean) were propagated in the higher range of soil moisture (>0.25 $m^3\ m^{-3}$) as compared to intermediate moisture classes (14–22%). The RMSE was more on DOY 323 (0.042 $m^3\ m^{-3}$) as compared to 339 (0.032 $m^3\ m^{-3}$). This could be due to a narrower NDVI range on former as compared to well-distributed NDVI on the later with little difference in the LST range between two dates (11 K on 18 November and 10 K on 4 December).

Since the LST–NDVI scatterplots showed non-linear trends in the dry edges and sloping trends in the wet edges, seven case studies were carried out to estimate surface soil moisture from ASTER LST–NDVI scatterplots using the dry-wet edge combinations as set out in Table 5.

The error statistics (bias, MAE and RMSE) of surface soil moisture estimates with respect to *in situ* measurements are also summarized in Table 5. The smallest errors in estimates in terms of MAE (0.026 $m^3\ m^{-3}$) and RMSE (0.039 $m^3\ m^{-3}$) were obtained for

Table 4
Error statistics of ASTER derived field scale surface soil moisture estimates in cropped regions of Ludhiana district of Punjab.

θ_v class ($m^3\ m^{-3}$)	Bias ($m^3\ m^{-3}$)			MAE ($m^3\ m^{-3}$)			RMSE ($m^3\ m^{-3}$)		
	(I)	(II)	Pooled	(I)	(II)	Pooled	(I)	(II)	Pooled
0.0–0.15	0.006	0.026	0.0127	0.017	0.026	0.020	0.027 (20%)	0.030 (24%)	0.028 (22%)
0.151–0.25	−0.020	−0.020	−0.020	0.021	0.020	0.020	0.031 (16%)	0.024 (12%)	0.028 (14%)
>0.25	−0.133	−0.042	−0.064	[a]	0.042	0.042	[a]	0.047 (17%)	0.078 (28%)
Pooled	−0.017	−0.014	−0.016	0.027	0.026	0.026	0.042 (25%)	0.032 (16%)	0.039 (20%)

[a] Only one sample was there in this class and that's why MAE and RMSE were not computed. (I) DOY 305 (18 November 2004); (II) DOY 339 (4 December 2004)
Bias $= (1/n)(P_i - O_i)$, MAE = Mean absolute error $\frac{1}{n}\sum(|P_i - O_i|)$, RMSE = root mean square error $= \left[\frac{1}{n}\sum (P_i - O_i)^2\right]^{1/2}$
Where, O_i and P_i, are measured and estimated θ_v, respectively. n is the number of paired datasets (30).

Table 5
Case studies on error analysis of field scale soil moisture estimates using different combinations of dry and wet edge approximations from LST– NDVI space using ASTER data.

Serial number	Cases	Bias ($m^3\ m^{-3}$)	MAE ($m^3\ m^{-3}$)	RMSE ($m^3\ m^{-3}$)
1	Linear dry edge and horizontal wet edge as per SWI definition	−0.016	0.026	0.039
2	Non-linear (2nd order polynomial fit of maximum LST to NDVI) dry edge and sloping wet edge as linear fit of minimum LST to NDVI	−0.020	0.035	0.047
3	Non-linear (2nd order polynomial fit of maximum LST to NDVI) dry edge and horizontal wet edge as per SWI definition	−0.026	0.036	0.051
4	Non-linear (3rd order polynomial fit of maximum LST to NDVI) dry edge and sloping wet edge as linear fit of minimum LST to NDVI	−0.010	0.032	0.043
5	Non-linear (3rd order polynomial fit of maximum LST to NDVI) dry edge and horizontal wet edge as per SWI definition	−0.021	0.035	0.050
6	Non-linear (4th order polynomial fit of maximum LST to NDVI) dry edge and sloping wet edge as linear fit of minimum LST to NDVI	−0.010	0.031	0.042
7	Non-linear (4th order polynomial fit of maximum LST to NDVI) dry edge and horizontal wet edge as per SWI definition	−0.021	0.034	0.049

case 1 (linear dry edge and horizontal wet edge) as compared to other cases when RMSE varied between 0.042 and 0.051 $m^3\ m^{-3}$.

6.2.2. Landscape scale

The surface soil moisture estimates were generated over four different agricultural landscapes using MODIS AQUA LST–NDVI scatterplots. Table 6 summarizes the validation statistics (mean bias, MAE, RMSE, r) of MODIS AQUA θ_v estimates over study regions for different soil moisture classes (0–0.15, 0.151–0.25 and >0.25 $m^3\ m^{-3}$) as well as with pooled datasets. Range of RMSE was found to be the highest (36–39% of measured mean) in θ_v class <0.15 $m^3\ m^{-3}$ followed by 8–18% and 12–23% for θ_v class 0.151–0.25 $m^3\ m^{-3}$ and >0.25 $m^3\ m^{-3}$, respectively. Temporal variations in bias from MODIS AQUA soil moisture estimates are shown in Fig. 7a–d. Errors in θ_v estimates were also computed for four NDVI classes: <0.35, 0.35–0.5, 0.5–0.65 and > 0.65. The RMSE were found to be higher (0.024 $m^3\ m^{-3}$) in low (<0.35) and high (>0.65) NDVI classes as compared to the two intermediate classes where these were 0.014 and 0.02 $m^3\ m^{-3}$, respectively. Goetz (1997) reported that the LST–NDVI triangular relationship is largely determined by fractional vegetation cover. The uncertainty of SWI is larger at high fractional vegetation cover where the wetness isolines are closely set (Sandholt et al., 2002). This is due to the fact that most of the soil is obscured at high fractional vegetation cover. Thus, the lower part of the triangle is an area where the errors in the inferred soil moisture content will be the largest. Therefore, Gillies and Carlson (1995) suggested that reliable results may be obtained by limiting evaluation of soil moisture to the range of fractional vegetation cover between 0 and 80%. The relative estimation error of SWI also increases at low fractional vegetation cover because the 'wet edge' is modelled as a horizontal base of the triangle as opposed to a sloping wet edge in the trapezoid approach (Moran et al., 1994). The 1:1 validation plot of MODIS θ_v estimates and *in situ* measurements (Fig. 8) with pooled datasets (n = 150)

Table 6
Error statistics of MODIS AQUA derived landscape surface soil moisture estimates in cropped regions.

Study regions	Soil moisture class ($m^3\ m^{-3}$)	Bias ($m^3\ m^{-3}$)	MAE ($m^3\ m^{-3}$)	RMSE ($m^3\ m^{-3}$)
(a) Punjab (Ludhiana, Moga, Ferozpur, Jalandhar, Kapurthala, Amritsar, Patiala)	0–0.15	0.031	0.030	0.043 (39%)
	0.151–0.25	0.007	0.020	0.024 (12%)
	>0.25	−0.041	0.042	0.050 (18%)
	Pooled (n = 82)	0.0036	0.028	0.036 (19%)
(b) Haryana (Hissar)	Pooled (n = 12)	−0.005	0.010	0.015 (10%)
(c) Orissa (Dhenkanal)	0–0.15	0.036	0.036	0.038 (34%)
	0.151–0.25	−0.0009	0.011	0.015 (8%)
	>0.25	N.A.	N.A.	N.A.
	Pooled (n = 24)	0.014	0.022	0.028 (17%)
(d) Karnataka (Bijapur)	0–0.15	0.001	0.019	0.025 (36%)
	0.151–0.25	−0.016	0.037	0.044 (23%)
	>0.25	−0.011	0.018	0.021 (8%)
	Pooled (n = 32)	−0.0046	0.025	0.032 (27%)

n: number of datasets; N.A. – not available.

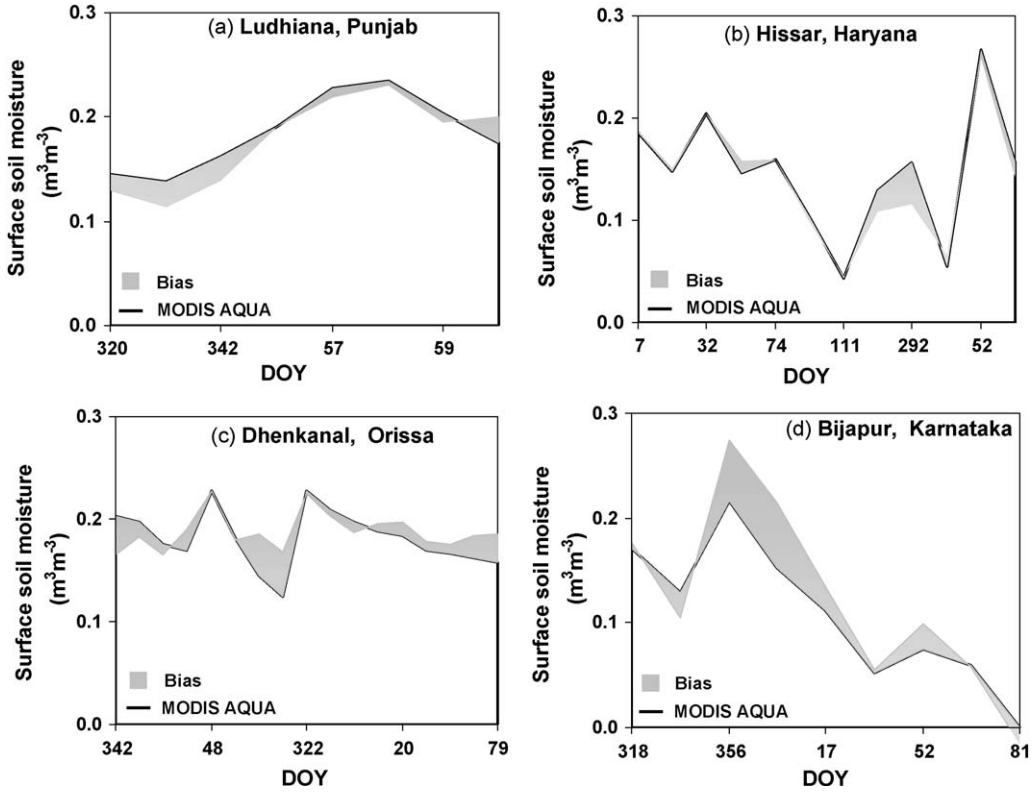

Fig. 7. Temporal evolution of landscape scale surface soil moisture estimates from MODIS AQUA and its bias over four different study regions.

yielded an overall RMSE of 0.033 $m^3\ m^{-3}$ (20% of measured mean) with $r = 0.88$ (significant at 5% level).

6.3. Evaluating present estimation errors in light of work done elsewhere

Field scale soil moisture retrieval by Thonfield and Schönermark (1998) using LANDSAT TM data and validation results in Germany showed an RMS error of 0.046 $m^3\ m^{-3}$ with a correlation coefficient of 0.87. They also reported that a dynamic range of NDVI is a pre-requisite for realistic estimation of soil moisture based on LST–NDVI relationship. Recent studies by Thoma et al. (2008) reported RMSE in the range of 0.03–0.18 $m^3\ m^{-3}$ with varying spatial scales between 21 and 49 m using active microwave C-band backscatter HH polarized data from RADARSAT SAR over three watersheds of Arizona, Oklahoma and Georgia. While estimating surface soil moisture using L-band radiometry over grass and alfalfa fields of Beltsville (Maryland, USA), ETH (Zurich, Switzerland) and SMOSREX (Tolouse, France) sites, Saleh et al. (2007) obtained a RMSE range of 0.015–0.120 $m^3\ m^{-3}$ at different polarization ratios. While estimating surface soil moisture over AMMA (African Monsoon Multidisciplinary Analysis) Sahelian site in Mali using ENVISAT/ASAR, Baup et al. (2007) obtained the lowest RMSE of 2.8% with low incidence angles and by taking into account vegetation effects using multi-angular radar data. For field scale soil moisture estimation, the errors in the present study are comparable with those obtained through other international studies conducted in different parts of the world using satellite data.

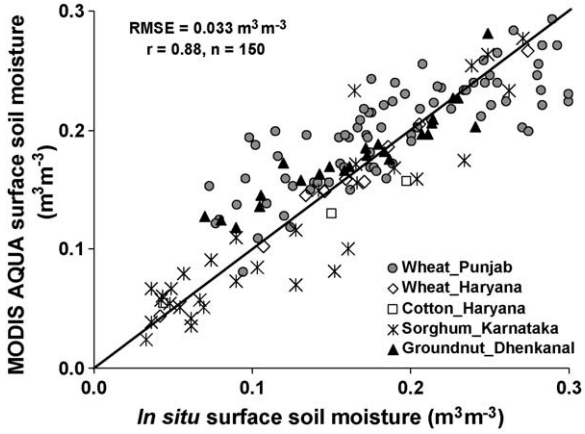

Fig. 8. Validation of landscape scale surface soil moisture estimates over different cropped sites with *in situ* measurements.

Earlier studies (Sandholt et al., 2002) compared the spatial pattern of AVHRR dryness index and simulated soil moisture from a distributed hydrological model, MIKE SHE, over northern Senegal at landscape scale. It produced maximum r-values of 0.9, but no direct estimation of θ_v was carried out. In China, significant negative correlation ($r = 0.35$–0.68) between dryness index and surface soil moisture was also found (Wang et al., 2004). A close match (negative correlation) in temporal variation of NOAA PAL (Pathfinder AVHRR Land) 10-day dryness index and 10-day cumulative rainfall was revealed by Bhattacharya et al. (2004) both in a drought and a normal year over a semi-arid region of North-Western India. The present work is the first exhaustive study to estimate volumetric soil moisture using such a large number of MODIS scenes and to validate with *in situ* measurements over a variety of agricultural landscapes.

6.4. Cross-scale comparison of soil moisture estimates from LST–NDVI space and uncertainty assessment

The error analysis of soil moisture estimates with respect to measurements revealed that the absolute overall RMSE was somewhat higher (0.039 $m^3\ m^{-3}$) (Table 4) at field scale than at

landscape scale (0.033 $m^3 m^{-3}$). The validation at field scale could be done only over one study region (i.e. Punjab) with 30 measurements as compared to four study regions for validation of landscape scale estimates with 150 measurements. Apart from that, with the finer resolution ASTER sensor, a smaller land area could be covered within the sampling window size due to its narrow swath (~60 km). This may often fail to represent dynamic ranges of NDVI and LST to produce required spatial heterogeneity in fractional cover and thermal conditions. Good dynamic ranges of these two surface variables are pre-conditions to obtain representative wetness patterns. It was already shown (Section 6.2.1) that errors in field scale soil moisture estimates become less with well-distributed NDVI having similar LST range within the same sampling window. ASTER derived field scale θ_v on DOY 323 and 339 were compared with those of MODIS TERRA instead of AQUA to ensure the same overpass time. The θ_v from ASTER sub-pixels within a MODIS pixel at all *in situ* soil moisture sampling locations in Punjab were linearly aggregated up to MODIS resolution. Aggregated ASTER θ_v were found to show a mean bias, mean absolute deviation (MAD) and root mean square deviation (RMSD) of −0.025, 0.043 and 0.054 $m^3 m^{-3}$. The RMSD of cross-scale comparison was slightly higher than the RMSE of estimates with respect to measurements at both the scales (field and landscape). The uncertainties in addition to inherent errors may have certain other causes. Sub-pixel heterogeneity at field scale may arise from differences in leaf geometry and orientation as well as terrain topographical differences. This heterogeneity is smoothed out during aggregation. The magnitude of loss of sub-pixel heterogeneity depends on target resolution. Scaling error through direct aggregation gets minimized when the spatial autocorrelation of a geophysical quantity at native resolution increases. A geostatistical technique was applied to assess sub-pixel heterogeneity of θ_v at field scale. The ranges of autocorrelation were equivalent to 4–5 ASTER resampled pixels and were less than half of MODIS resampled pixel resolution. This could be one of the additional sources of uncertainties of θ_v for cross-scale comparison of estimates apart from inherent sources of errors mentioned earlier. Since LST and NDVI are sole quantities to derive SWI and θ_v, the sub-pixel ASTER LST and NDVI within MODIS TERRA pixel at all *in situ* measurement sites in Punjab were aggregated up to target MODIS resolution. The MAD and RMSD of aggregated ASTER LST and NDVI were found to be 2.76 K, 3.16 K and 0.095, 0.127, respectively as compared to MODIS TERRA. These differences between basic quantities could also produce moisture differences while scaling. Liu et al. (2006) used different aggregation techniques on ASTER LST by using a digital elevation model (DEM) to incorporate slope and aspects while aggregating to MODIS TERRA resolution. Comparison of aggregation techniques yielded best LST RMSD of 1.87 K. The inherent accuracy of LST retrieval is also associated with assignment of surface emissivity, which is based on LUT (look-up table) in case of MODIS. In ASTER, the NEM (normalized emissivity method), ratio and MMD (maximum–minimum difference) modules were used for surface emissivity determination. The difference in NDVI retrieval from surface reflectances in red and near-infrared bands is also another source of uncertainty for SWI determination in addition to inherent error sources in LST retrieval. MODIS atmospheric spatial products such as ozone, precipitable water and aerosol were used as inputs to atmospheric radiative transfer scheme to convert at-sensor reflectance to surface reflectance. In ASTER, only standard or reference atmospheric profiles were used to generate surface reflectance. This may not represent real atmospheric conditions on ASTER overpass dates. These could also lead to differences in NDVI between ASTER and MODIS on the same date, or a certain level of discrepancy could also occur between two close overpass days for the same sensor.

6.5. Comparison of θ_v from LST–NDVI triangle with global scale estimates from passive microwave radiometry

6.5.1. Temporal evolution of θ_v estimates over contrasting agroecosystems

Passive microwave remote sensing provides a unique capability of obtaining daily large-area soil moisture estimates at global and regional scales (Njoku and Entekhabi, 1996). Moreover, the retrieved output using the data from a C-band passive microwave sensor (AMSR-E) in the AQUA platform is the only operational large-scale soil moisture product (AE_Land) available globally (Njoku et al., 2003). The θ_v from SWI were computed using 28 eight-day MODIS AQUA LST and NDVI. These were aggregated to AMSR-E grids over two contrasting agroecosystems of Ludhiana (Punjab) and Bijapur (Karnataka) between November 2005 and May 2006. Cereal crops with maximum canopy height of 0.90 m are dominant during *rabi* season in the sub-humid climate of Ludhiana. The sorghum with maximum canopy height of 2.5 m is dominant in the semi-arid climate of Bijapur. Similarly, eight-day average AMSR-E θ_v was computed over those grids from its daily values. Time series of these two for the same period are plotted in Fig. 9a and b. Maximum differences in θ_v between MODIS and AMSR-E occurred during maximum agricultural growth and the differences decreased at the beginning and end of a growing season. Over Ludhiana (Punjab), a significant discrepancy in θ_v between the two sensors was observed between DOY 17 and 65 (17 January 2006 to 6 March 2006) when *rabi* crops (e.g. largely wheat) undergo active vegetative and reproductive phases. Over Bijapur (Karnataka), maximum difference in θ_v was observed during 305–361 DOY (1 November 2005 to 27 December 2005) when *rabi* crops (e.g. sorghum–sunflower combinations in large area) were at active vegetative growth stage. However, this

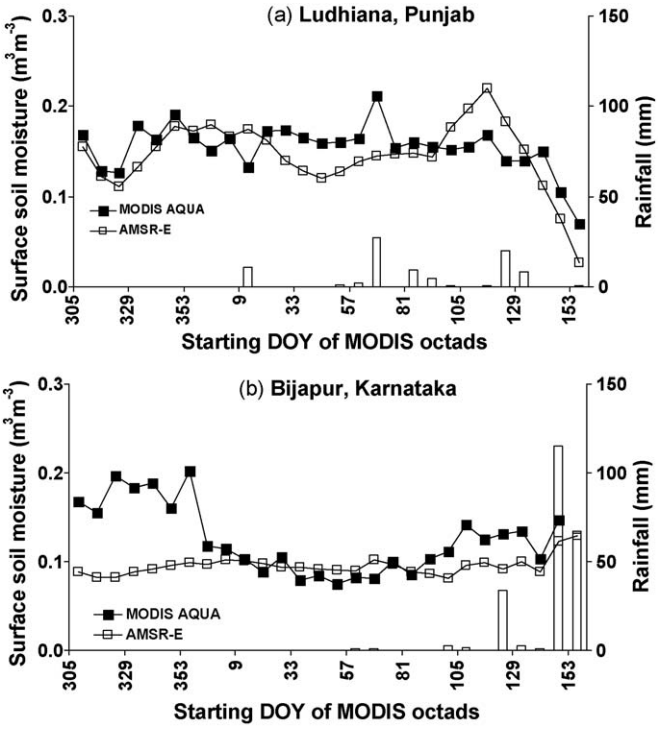

Fig. 9. Temporal comparison of MODIS AQUA eight-day landscape scale and AMSR-E global scale surface soil moisture estimates from DOY 305 (1 November 2005) to DOY 153 (31 May 2006) in the validation sites of (a) Ludhiana, Punjab and (b) Bijapur, Karnataka. The lines indicate variation of satellite based surface soil moisture estimates. The bars indicate variation of measured rainfall in the validation sites during the same period.

Table 7
Comparison of surface soil moisture estimates between aggregated MODIS AQUA and AMSR-E for different fractional vegetation cover classes.

Fractional vegetation cover class	Mean deviation ($m^3\ m^{-3}$)	MAD ($m^3\ m^{-3}$)	RMSD ($m^3\ m^{-3}$)	r
Less than 0.5	0.008	0.023	0.027 (22%)	0.75
Greater than 0.5	0.042	0.050	0.060 (36%)	−0.47

MAD: mean absolute deviation; RMSD: root mean square deviation. Mean deviation, MAD and RMSD are used when comparison of surface soil moisture estimates were carried out between MODIS AQUA and AMSR-E. Mean deviation $= (1/n)(P_i - O_i)$, MAD $= \frac{1}{n}\sum(|P_i - O_i|)$, RMSD $= \left[\frac{1}{n}\sum(P_i - O_i)^2\right]^{1/2}$
Where, O_i and P_i, are AMSR-E estimates and MODIS AQUA estimates, respectively. n is the number of paired datasets.

difference was reduced when the crops reached physiological maturity.

The presence of a vegetation layer above the soil surface alters microwave emission in two ways: (1) it attenuates the energy emitted by the soil and (2) it adds an emission component of its own. Part of this component is emitted by the vegetation directly upward into the air; another part is initially emitted downward towards the soil surface and then, upon reflection by the surface, propagates upward through the vegetation layer into the air (Jackson and Schmugge, 1991). The vegetation layer introduces a masking effect, reducing the sensitivity of the microwave radiometer to soil moisture (Loew, 2008). The magnitude of this masking effect is dependent on the structure and wet biomass of the vegetation layer. The results were further investigated for the influence of surface roughness on microwave retrieval of θ_v. MODIS AQUA eight-day fAPAR (assumed equivalent to fractional vegetation cover, F_v) were used as surrogate for vegetation roughness (Basist et al., 2001). Error analysis of θ_v between two scales was carried out for two F_v classes ($\leq$0.5 and >0.5). Error statistics of θ_v estimates between MODIS and AMSR-E for two F_v classes are given in Table 7. The mean bias, mean absolute deviation (MAD) and root mean square deviation of θ_v estimates for F_v class <0.5 were 0.008 $m^3\ m^{-3}$, 0.023 $m^3\ m^{-3}$, 0.027 $m^3\ m^{-3}$ (22% of measured mean), respectively with positive correlation (r = 0.75). On the contrary, these values were 0.042 $m^3\ m^{-3}$, 0.05 $m^3\ m^{-3}$, 0.06 $m^3\ m^{-3}$ (36% of measured mean), respectively with negative correlation (r = −0.47) for F_v > 0.5. Moreover, it was also observed that differences in θ_v were significantly higher in Bijapur during the active vegetative stage of sorghum–sunflower combinations as compared to differences in active vegetative stage in wheat over Punjab. Surface roughness increases with crop height. Crop height attains its maximum at peak vegetative stage. Maximum crop height of sorghum (~2.5 m) is more than wheat (~0.9 m). This increased the surface roughness that contaminates soil moisture signals sensed by microwave radiometer (Wang, 1985; Njoku and Chan, 2006). It was also noticed that, for F_v class <0.5, the correlation between two sources of θ_v estimates from different scales was higher (80%) in Ludhiana than in Bijapur. This could be attributed to possibly higher spatial autocorrelation of AQUA θ_v in sub-grids within one AMSR-E grid due to less heterogeneity in Ludhiana (Punjab) as compared to Bijapur (Karnataka).

6.5.2. Intercomparison of soil moisture distribution pattern in agroecosystems

Spatial distributions of surface soil moisture (both from optical–thermal and microwave sensors) over agroecosystems in Punjab and Karnataka state are shown in Figs. 10 and 11. Spatial patterns matched quite well during the period of low vegetation activity (Figs. 10a and 11b) in contrast to peak growth stages (Figs. 10b and 11a). In Punjab, the spatial pattern of surface soil moisture from the two sensors showed close resemblance on DOY 331 (26 November 2004) because the surface condition was almost fallow (after crop harvest) or in the emergence stage of *rabi* crops (e.g. wheat). On the contrary, there was a poor spatial coherence

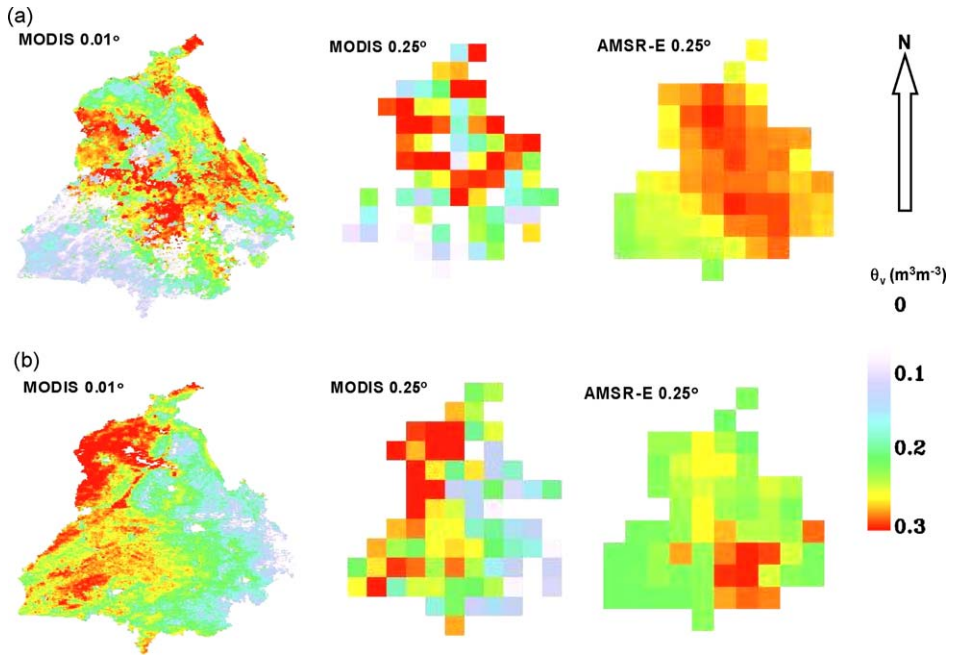

Fig. 10. (a) Spatial distribution of surface soil moisture from MODIS AQUA (at 0.01° and 0.25°) and AMSR-E (0.25°) over Punjab state on DOY 331 (26 November 2004) with low vegetation cover condition; (b) Spatial distribution of surface soil moisture from MODIS AQUA (at 0.01° and 0.25°) and AMSR-E (0.25°) over Punjab state on DOY 61 (2 March 2005) with high vegetation cover condition.

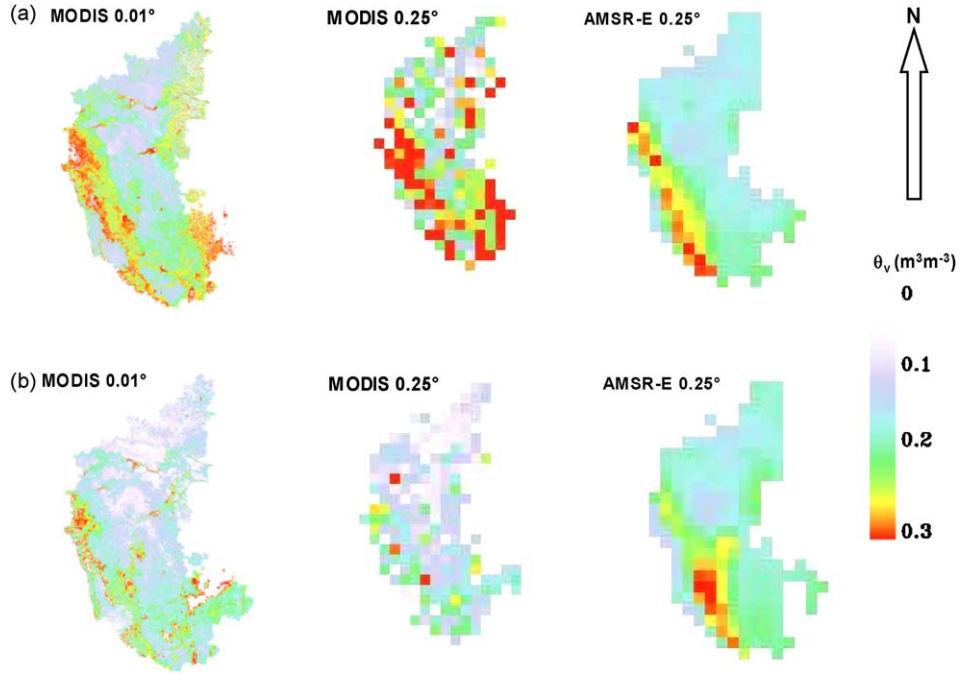

Fig. 11. (a) Spatial distribution of surface soil moisture from MODIS AQUA (at 0.01° and 0.25°) and AMSR-E (0.25°) over Karnataka state on DOY 354 (20 December 2005) with high vegetation cover condition, (b) Spatial distribution of surface soil moisture from MODIS AQUA (at 0.01° and 0.25°) and AMSR-E (0.25°) over Karnataka state on DOY 52 (21 February 2006) with low vegetation cover condition.

between MODIS AQUA and AMSR-E θ_v on DOY 61 (2 March 2005) because *rabi* crops were at peak growth stage. Effect of surface roughness on microwave emission was responsible for this typical difference. Similarly, in Karnataka state, a poor spatial match of θ_v between the two sensors was evident on DOY 354 (20 December 2005) due to *rabi* crops (sorghum + sunflower) being at their peak growth.

Measurements at higher microwave frequencies in the C-band range (~4–8 GHz) have been shown to be sensitive to soil moisture, but primarily in the region of low vegetation (Jackson et al., 2002). The increased attenuation by vegetation and the shallow sensing depth at C-band impose limitations on the retrieval of soil moisture by AMSR-E. Vegetation and roughness effects become more pronounced as the frequency increases: hence low frequencies (high wavelength) in the L-band range (~1–2 GHz) are preferred for soil moisture sensing. Furthermore, at lower microwave frequencies such as L-band, the soil emission originates from deeper layer in the soil (a few centimeters), giving a more representative measurement of moisture conditions below the surface layer.

6.5.3. Scale issues

Terrain parameters such as slope, aspect and relative proportion of land cover types and soil types are the sources of landscape heterogeneity. It is expected that direct aggregation of MODIS θ_v estimates within AMSR-E sub-grids may propagate errors while scaling. A semi-variance analysis was conducted with MODIS AQUA θ_v estimates at 0.01° grid resolution to characterize its spatial autocorrelation. The semivariogram parameters (nugget, sill and range) from an exponential model derived on some of the selected *in situ* moisture measurement dates are summarized in Table 8. It was found that the range of spatial autocorrelation was relatively higher over Punjab as compared to Karnataka. It varied between 12 and 18 MODIS resampled pixels for soil moisture within Ludhiana and adjacent areas. But it was less (between 7 and 12 MODIS resampled pixels) in Bijapur and adjacent regions. The better autocorrelation of θ_v in Ludhiana at landscape scale produced low overall RMSD (0.031 $m^3 m^{-3}$) as compared to Bijapur (RMSD = 0.05 $m^3 m^{-3}$) through comparison of eight-day soil moisture from optical–thermal and passive microwave sensing.

Table 8
Semivariogram statistics of MODIS AQUA derived surface soil moisture on selected dates throughout a crop growing period.

Study region	DOY (date) of analysis	Nugget	Sill	Range[a] (in MODIS resampled pixels)
Punjab	280 (9 October 2004)	0.00037	0.00169	17
	308 (3 November 2004)	0.00032	0.00139	17
	344 (10 December 2004)	0.00039	0.00143	15
	34 (3 February 2005)	0.00046	0.00145	12
	61 (2 March 2005)	0.00020	0.00150	18
	102 (12 April 2005)	0.00015	0.00080	17
Karnataka	319 (15 November 2005)	0.00061	0.00144	10
	342 (8 December 2005)	0.00062	0.00146	12
	3 (3 January 2006)	0.00074	0.00198	10
	39 (8 February 2006)	0.00061	0.00130	9
	66 (7 March 2006)	0.00121	0.00263	7

[a] One resampled MODIS pixel for estimated soil moisture = 0.01°.

7. Summary and conclusions

The present study demonstrated the technique of using surface temperature–vegetation index triangular space to derive a soil wetness index to estimate volumetric surface moisture (θ_v) content in cropped soils at field and landscape scales over selected agricultural regions of India. The dry and wet edges extracted from LST–NDVI space were used to derive SWI. Non-linear trends in the dry edge at higher NDVI and a sloping wet edge were found in the case of ASTER LST–NDVI scatters. The possible reasons could be (i) the attenuation of upwelling longwave radiation from background soil caused by dominant proportion of sunlit canopy at field scale as compared to shaded ones at higher NDVI (Carlson et al., 1990) and (ii) prominent effect of asymptotic increase of NDVI followed by saturation at LAI between 2 and 6 at field scale (Carlson and Ripley, 1997) than landscape scale. However, among different types of combinations of dry and wet edges, the assumption of the combination of a linear dry edge and horizontal wet edge yielded best results. Relatively well-developed triangles from LST–NDVI scatters with sharp dry and wet edges were found in case of MODIS AQUA. The landscape heterogeneity, largely governed by cover fraction from lumped canopies, generally smoothens the influence of sunlit-shaded canopy proportioning. It has been found that enhanced vegetation index (EVI) determined from combinations of blue, red and near-infrared band reflectances can capture higher LAI better than NDVI (Chen et al., 2004). Future attempts should aim at generating SWI from LST–EVI 2D space to better estimate surface soil moisture at all LAI classes irrespective of spatial scales. Validation of field scale θ_v estimates from ASTER produced a RMSE of 0.039 $m^3\ m^{-3}$ (20% of measured mean) with pooled ($n = 30$) datasets. This study showed that the validity of surface moisture estimates largely depends on dynamic ranges of LST and NDVI, which often may not be sufficient as a result of restricted sampling window size due to low swath in case of finer resolution sensors. This finding is in agreement with the observation that the effectiveness of LST–NDVI triangles for soil moisture estimation increases as the surface heterogeneity increases in a sampling domain. The greater dynamic ranges of these two surface variables from a desired sampling window for larger swath by moderate resolution sensor could lead to relatively low overall RMSE (0.033 $m^3\ m^{-3}$, 20% of measured mean) in landscape scale θ_v estimates. The errors were less for the intermediate NDVI range, 0.35–0.65, than for the lower (<0.35) and higher (>0.65) NDVI intervals. The errors of both field and landscape scale estimates were least at intermediate soil moisture class (0.15–0.25 $m^3\ m^{-3}$) as compared to lower (0–0.15 $m^3\ m^{-3}$) and higher classes (>0.25 $m^3\ m^{-3}$). In addition to inherent sources of errors, degree of field scale heterogeneity in soil moisture within a landscape and differences in techniques used to retrieve LST and NDVI from different sensors but with same overpass time appeared to be the other sources of uncertainties for cross-scale comparison of θ_v estimates. However, the overall errors of estimates at both scales were found to be comparable with the best validation results available worldwide for soil moisture estimation using satellite data. Time series comparison of eight-day θ_v from MODIS AQUA LST–NDVI triangle was made with large-area global scale estimates through passive microwave radiometer from AMSR-E over two large contrasting agroecosystems at Ludhiana and Bijapur. This revealed a fairly good correlation (0.75) and low RMSD of 0.027 $m^3\ m^{-3}$ for fractional vegetation cover (F_v) below 0.5. At high fractional cover, microwave sensing of soil moisture with longer frequency (C-band) is hindered by high surface roughness. The higher canopy height of cover types also causes greater deviation due to influence of increased roughness on microwave signal than soil wetness. Moreover, it appeared from the analysis that surface soil moisture estimates from passive microwave produced low errors at low vegetation cover with higher frequency in C-band range. Thus, low frequency in the L-band range is preferred for soil moisture sensing with less influence of surface roughness. The LST–NDVI triangle method showed less error for the intermediate NDVI range 0.35–0.65. A synergistic use of shorter microwave frequency (L-band) and optical–thermal infrared data for the estimation of surface soil moisture at high resolution was evaluated by Chauhan et al. (2003) and it will be applied to National Polar-Orbiting Operational Environmental Satellite System (NPOESS), planned for launch in the 2009–2010 time frame by NASA (National Aeronautics and Space Administration).

Acknowledgements

This study was carried out in the project titled "Energy and Water Balance Monitoring from Geostationary Platform for Agricultural Applications" between 2002 and 2007 under Earth Observation Application Missions (EOAM) funded by Department of Space (DOS), India. We are thankful to Dr. Sushma Panigrahy, Group Director, Agriculture-Forestry and Environment Group and Dr. J.S. Parihar, Deputy Director, Remote Sensing Applications Area (RESA) for providing facilities during the study. We duely acknowledge the constant encouragement by Dr. R.R. Navalgund, Director, Space Applications Centre during the course of this study. Authors are grateful to Prof. Steven Running, Director, Numerical Terradynamic Simulation Group (NTSG), Montana for his valuable suggestions while carrying out this study. We also thank anonymous reviewers for their critical comments and wonderful suggestions that substantially improved the clarity of this paper.

References

Basist, A., Williams, C., Grody, N., Ross, T.F., Shen, S., Chang, A.T.C., Ferraro, R., Menne, M.J., 2001. Using the spatial sensor microwave imager to monitor surface wetness. J. Hydrometeorol. 2, 297–308.

Baup, F., Mougin, E., de Rosnay, P., Timouk, F., Chênerie, I., 2007. Surface soil moisture estimation over the AMMA Sahelian site in Mali using ENVISAT/ASAR data. Remote Sens. Environ. 109, 473–481.

Beljaars, A., Viterbo, P., Miller, M., Betts, A., 1996. The anomalous rainfall over the United States during July 1993: sensitivity to land surface parameterization and soil moisture anomalies. Monthly Weather Rev. 124, 362–383.

Betts, A.K., Ball, J.H., 1998. FIFE surface climate and site-average dataset 1987-89. J. Atm. Sci. 55, 1091–1108.

Bhattacharya, B.K., Yong, K.Y., Dadhwal, V.K., 2004. Characterizing surface moisture availability using NOAA AVHRR coarse resolution vegetation index and thermal data. J. Agromet. 6, 191–196.

Brubaker, L., Entekhabi, D., 1996. Analysis of feedback mechanisms in land-atmosphere interaction. Water Resour. Res. 32, 1343–1357.

Cahill, A.T., Parlange, M.B., Jackson, T.J., O'Neill, P., Schmugge, T.J., 1999. Evaporation from nonvegetated surfaces: surface aridity methods and passive microwave remote sensing. J. Appl. Meteorol. 38 (9), 1346–1351.

Capehart, W.J., Carlson, T.N., 1997. Decoupling of surface and near-surface soil water content: a remote sensing perspective. Water Resour. Res. 33 (6), 1383–1395.

Carlson, T.N., Perry, E.M., Schmugge, T.J., 1990. Remote estimation of soil moisture availability and fractional vegetation cover for agricultural fields. Agric. For. Meteorol. 52, 45–69.

Carlson, T.N., Gillies, R.R., Schmugge, T.J., 1995. An interpretation of methodologies for indirect measurement of soil water content. Agric. For. Meteorol. 77, 191–205.

Carlson, T.N., Ripley, D.A., 1997. On the relation between NDVI, fractional vegetation cover, and leaf area index. Remote Sens. Environ. 62, 241–252.

Carlson, T.N., 2007. Review: an overview of the "triangle method" for estimating surface Evapotranspiration and soil moisture from satellite imagery. Sensors 7, 1612–1629.

Chauhan, N.S., Miller, S., Ardauny, P., 2003. Spaceborne soil moisture estimation at high resolution: a microwave-optical/IR synergistic approach. Int. J. Remote Sens. 24 (22), 4599–4622.

Chen, X., Vierling, L., Rowell, E., DeFelice, T., 2004. Using lidar and effective LAI data to evaluate IKONOS and Landsat 7 ETM + vegetation cover estimates in a ponderosa pine forest. Remote Sens. Environ. 91, 14–26.

Cosh, M.H., Jackson, T.J., Bindlish, R., Prueger, J.H., 2004. Watershed scale temporal and spatial stability of soil moisture and its role in validating satellite estimates. Remote Sens. Environ. 92, 427–435.

de Rosnay, P., Calvet, J.C., Kerr, Y., Wigneron, J.P., Lemaître, F., Escorihuela, M.J., Sabater, J.M., Saleh, K., Barrie, J., Bouhours, G., Coret, L., Cherel, G., Dedieu, G.,

Durbe, R., Fritz, N.E.D., Froissard, F., Hoedjes, J., Kruszewski, A., Lavenu, F., Suquia, D., Waldteufel, P., 2006. SMOSREX: A long term field campaign experiment for soil moisture and land surface processes remote sensing. Remote Sens. Environ. 102, 377–389.

de Wit, A.J.W., van Diepen, A.J., 2007. Crop model data assimilation with the Ensemble Kalman filter for improving regional crop yield forecasts. Agric. For. Meteorol. 146, 38–56.

Dirmeyer, P.A., Zeng, F.J., Ducharne, A., Morrill, J.C., Koster, R.D., 2000. The sensitivity of surface fluxes to soil water content in three land surface schemes. J. Hydrometeorol. 1 (2), 121–134.

Eltahir, E.A.B., 1998. A soil moisture rainfall feedback mechanism 1 Theory and observations. Water Resour. Res. 34 (4), 765–776.

Entekhabi, D., 1995. Recent advances in land-atmosphere interaction research. Rev. Geophys. 33 (S1), 995–1004.

FAO/UNESCO, 1974. FAO/UNESCO Soil Map of the World, 1:5,000,000, ten volumes.

Fensholt, R., Sandholt, I., 2003. Derivation of a shortwave infrared water stress index from MODIS near- and shortwave infrared data in a semiarid environment. Remote Sens. Environ. 87, 111–121.

Friedl, M.A., Davis, F.W., 1994. Sources of variation in radiometric surface temperature over a tallgrass praire. Remote Sens. Environ. 48, 1–17.

Gillies, R.R., Carlson, T.N., 1995. Thermal remote sensing of surface soil water content with partial vegetation cover for incorporation into climate models. J. Appl. Meteorol. 34, 745–756.

Goetz, S.J., 1997. Multi-sensor analysis of NDVI, surface temperature and biophysical variables at mixed grassland site. Int. J. Remote Sens. 18 (1), 71–94.

Guerif, M., Duke, C.L., 2000. Adjustment procedures of a crop model to the site-specific characteristics of soil and crop using remote sensing data assimilation. Agric. Ecosyst. Environ. 81 (1), 57–69.

Hayden, C.M., Wales, E.S., Schmit, T.I., 1996. Derived product imagery from GOES-8. J. Appl. Meteorol. 35, 153–162.

Jackson, R.D., Reginato, R.J., Idso, S.B., 1977. Wheat canopy temperature: a practical tool for evaluating water requirements. Water Resour. Res. 13, 651–656.

Jackson, T.J., Schmugge, T.J., 1991. Vegetation effects on the microwave emissions of soils. Remote Sens. Environ. 36, 203–212.

Jackson, T.J., Gasiewski, A.J., Oldak, A., Klein, M., Njoku, E.G., Yevgrafov, A., Chistiani, S., Bindlish, R., 2002. Soil moisture retrieval using the C-band polarimetric scanning radiometer during the Southern Great Plains. IEEE Trans. Geos. Remote Sens. 2151–2161.

Jackson, T.J., Bindlish, R., Gasiewski, A.J., Stankov, B., Klein, M., Njoku, E.G., Bosch, D., Coleman, T.L., Laymon, C.A., Starks, P., 2005. Polarimetric scanning radiometer C- and X-band microwave observations during SMEX03. IEEE Trans. Geosci. Remote Sens. 43 (11), 2418–2430.

Jacobs, J.M., Mohanty, B.P., Hsu, E.-C., Miller, D., 2004. SMEX02: field scale variability, time stability and similarity of soil moisture. Remote Sens. Environ. 92, 436–446.

Kerr, Y.H., Waldteufel, P., Wigneron, J.P., Martinuzzi, J.M., Font, J., Berger, M., 2001. Soil moisture retrieval from space: The Soil Moisture and Ocean Salinity (SMOS) mission. IEEE Trans. Geosci. Remote Sens. 39, 1729–1735.

Khanna, S., Orueta, A.P., Whiting, M.L., Ustin, S.L., Riaño, D., Litago, J., 2007. Development of angle indexes for soil moisture estimation, dry matter detection and land-cover discrimination. Remote Sens. Environ. 109, 154–165.

Kustas, W.P., Hatfield, J.H., Prueger, J.H., 2005. The soil moisture-atmosphere coupling experiment (SMACEX): background, hydrometeorological conditions, and preliminary findings. J. Hydrometeorol. 6 (6), 791–804.

Lambin, E.F., Ehrlich, D., 1995. Combining vegetation indices and surface temperature for land-cover mapping at broad spatial scales. Int. J. Remote. Sens. 16 (3), 573–579.

Lillesaeter, O., 1982. Spectral reflectance of partly transmitting leaves: laboratory measurements and mathematical modeling. Remote Sens. Environ. 12, 247–254.

Liu, Y., Hiyama, T., Yamaguchi, Y., 2006. Scaling of land surface temperature using satellite data: a case examination on ASTER and MODIS products over a heterogeneous terrain area. Remote Sens. Environ. 105 (2), 115–128.

Loew, A., 2008. Impact of surface heterogeneity on surface soil moisture retrievals from passive microwave data at the regional scale: The Upper Danube case. Remote Sens. Environ. 112, 231–248.

Monteith, J.L., 1981. Evaporation and surface temperature. Q. J. Roy. Met. Soc. 107, 1–27.

Moran, M.S., Clarke, T.R., Inoue, Y., Vidal, A., 1994. Estimating crop water déficit using the relationship between surface-air temperature and spectral vegetation index. Remote Sens. Environ. 49, 246–263.

Mueller, R.W., Dagestad, K.F., Ineichen, P., Schroedter-Homscheidt, M., Cros, S., Dumortier, D., Kuhlemann, R., Olseth, J.A., Piernavieja, G., Reise, C., Wald, L., Heinemann, D., 2004. Rethinking satellite-based solar irradiance modeling The SOLIS clear-sky module. Remote Sens. Environ. 91, 160–174.

Murray, T., Verhoef, A., 2007. Moving towards a more mechanistic approach in the determination of soil heat flux from remote measurements. I. A universal approach to calculate thermal inertia. Agric. For. Meteorol. 147, 80–87.

Nemani, R.R., Pierce, L., Running, S.W., Goward, S., 1993. Developing satellite derived estimates of surface moisture status. J. Appl. Meteorol. 32, 548–557.

Nemani, R.R., Running, S.W., 1997. Land cover characterization using multi-temporal red, near-IR and thermal-IR data from NOAA/AVHRR. Ecol. Appl. 7 (1), 79–90.

Njoku, E.G., Entekhabi, D., 1996. Passive remote sensing of soil moisture. J. Hydrol. 184, 57–84.

Njoku, E.G., Li, L., 1999. Retrieval of land surface parameters using passive microwave measurements at 6–18 GHz. IEEE Trans. Geosci. Remote Sens. 37, 79–93.

Njoku, E.G., Jackson, T.J., Lakshmi, V., Chan, T.K., Nghiem, S.V., 2003. Soil moisture retrieval from AMSR-E. IEEE Trans. Geosci. Remote Sens. 41 (2), 215–229.

Njoku, E.G., Chan, S.T., 2006. Vegetation and surface roughness effects on AMSR-E land observations. Remote Sens. Environ. 100, 190–199.

Rosema, A., Fiselier, J.L., 1990. Meteosat-based evapotranspiration and thermal inertia mapping for monitoring transgression in the Lake Chad region and Niger Delta. Int. J. Remote Sens. 11 (5), 741–752.

Saleh, K., Wigneron, J.P., Waldteufel, P., de Rosnay, P., Schwank, M., Calvet, J.C., Kerr, Y.H., 2007. Estimates of surface soil moisture under grass covers using L-band radiometry. Remote Sens. Environ. 109, 42–53.

Sandholt, I., Rasmussen, K., Andersen, J., 2002. A simple interpretation of the surface temperature/vegetation index space for assessment of surface moisture status. Remote Sens. Environ. 79, 213–224.

Shuttleworth, W.J., 1991. Insight from large-scale observational studies on land/atmosphere interactions. Land Surface-Atmosphere Interactions for Climate Modeling, Observations. In: Wood, E.F. (Ed.), Models and Analysis. Kluwer Academic, pp. 300–320.

Singh, R.P., Oza, S.R., Chaudhari, K.N., Dadhwal, V.K., 2005. Spatial and temporal patterns of surface soil moisture over India estimated using surface wetness index from microwave radiometer (SSM/I). Int. J. Remote Sens. 26, 1269–1276.

Smith, R.C.G., Choudhury, B.J., 1991. Analysis of normalized difference and surface temperature observations over southeastern Australia. Int. J. Remote Sens. 12 (10), 2021–2044.

Stisen, S., Sandholt, I., Nöörgard, A., Fensholt, R., Jensen, K.H., 2008. Combining the method with thermal inertia to estimate regional evapotranspiration-applied to MSG-SEVIRI data in the Senegal River basin. Remote Sens. Environ. 112, 1242–1255.

Thapliyal, P.K., Pal, P.K., Narayanan, M.S., 2005. Development of a time series-based methodology for estimation of large-area soil wetness over India using IRS-P4 microwave radiometer data. J. Appl. Meteorol. 44, 127–143.

Thoma, D.P., Moran, M.S., Bryant, R., Rahman, M.M., Holifield Collins, C.D., Keefer, T.O., Noriega, R., Osman, I., Skrivin, S.M., Tischler, M.A., Bosch, D.D., Starks, P.J., Peters-Lidard, C.D., 2008. Appropriate scale of soil moisture retrieval from high resolution radar imagery for bare and minimally vegetated soils. Remote Sens. Environ. 112 (2), 403–414.

Thonfield, H., Schönermark, M., 1998. Estimation of soil moisture under vegetation using multisensor data. In: Part of the EUROPTO Conference on Remote Sensing for Agriculture, Ecosystem, and Hydrology, Barcelona, Spain, September 1998 , SPIE, vol. 3499. pp. 20–29.

Verhoef, A., Van den Hurk, B.J.J.M., Jacobs, A.F.G., Heusinkveld, B.G., 1996. Thermal soil properties for a vineyard (EFEDA-I) and a savanna (HAPEX-Sahel) site. Agric. For. Meteorol. 78, 1–18.

Verstraeten, W.W., Veroustraete, F., van der Sande, C.J., Grootaers, I., Feyen, J., 2006. Soil moisture retrieval using thermal inertia, determined with visible and thermal spaceborne data validated for European forests. Remote Sens. Environ. 101, 299–314.

Vivoni, E.R., Gebremichael, M., Watts, C.J., Bindlish, R., Jackson, T.J., 2008. Comparison of ground-based and remotely-sensed surface soil moisture estimates over complex terrain during SMEX04. Remote Sens. Environ. 112 (2), 314–325.

Wagner, W., Lemoine, G., Rott, H., 1999. A method for estimating soil moisture from ERS scatterometer and soil data. Remote Sens. Environ. 70, 191–207.

Wang, C., Qi, S., Niu, Z., Wang, J., 2004. Evaluating soil moisture status in China using the temperature-vegetation dryness index (TVDI). Can. J. Remote Sens. 30 (5), 671–679.

Wang, K.C., Li, Z.Q., Cribb, M.M., 2006. Estimation of evaporative fraction from a combination of day and night land surface temperatures and NDVI: a new method to determine Priestley-Taylor parameter. Remote Sens. Environ. 102, 293–305.

Wang, J.R., 1985. Effect of vegetation on soil moisture sensing observed from orbiting microwave radiometers. Remote Sens. Environ. 17, 141–151.

Wetzel, P.J., Chang, J.T., 1988. Evaporation from non-uniform surfaces: a first approach for short-term numerical weather prediction. Monthly Weather Rev. 116, 600–621.

Wetzel, P.J., Woodward, R.H., 1987. Soil moisture estimation using GOES-VISSR infrared data: a case study with simple statistical method. J. Climate Appl. Meteorol. 26, 107–115.

Wilson, M.F., Henderson-Sellers, A., Dickinson, R.E., Kennedy, P.J., 1987. Sensitivity of the Biosphere-Atmosphere Transfer Scheme (BATS) to inclusion of variable soil characteristics. J. Climate Appl. Meteorol. 60, 341–362.